Chemical Engineering and Processing 82 (2014) 71–87

Contents lists available at ScienceDirect

Chemical Engineering and Processing: Process Intensification

journal homepage: www.elsevier.com/locate/cep

Kinetic and thermodynamic investigations of non-isothermal decomposition process of a commercial silver nitrate in an argon atmosphere used as the precursors for ultrasonic spray pyrolysis (USP): The mechanistic approach

Bojan Janković [a,*], Srećko Stopić [b], Jelena Bogović [b], Bernd Friedrich [b]

[a] Faculty of Physical Chemistry, Department for Dynamics and Matter Structure, University of Belgrade, Studentski trg 12-16, P.O. Box 137, 11001 Belgrade, Serbia
[b] IME Process Metallurgy and Metal Recycling, RWTH Aachen University, Aachen, Germany

ARTICLE INFO

Article history:
Received 18 December 2013
Received in revised form 13 May 2014
Accepted 2 June 2014
Available online 8 June 2014

Keywords:
Silver nitrate
Ultrasonic spray pyrolysis (USP)
Thermogravimetric analysis (TGA)
Critical temperature
Defects
Thermodynamic properties

ABSTRACT

The non-isothermal decomposition process of commercial silver nitrate used as the precursor for the USP procedure was investigated by simultaneous TGA–DTA measurements at different heating rates, in an argon atmosphere. Detailed kinetic and thermodynamic analyses, with special emphasis on the formation of a complete mechanistic scheme of the process were performed. It was found that the process under study can be described by the acceleratory power law kinetic model (P2), in the range of the extent of conversion (α) values ($0.15 \leq \alpha \leq 0.85$), where the value of the apparent activation energy (E_a) can be considered as the constant (141.3 kJ mol^{-1}). The kinetic prediction analysis was shown that only the power law kinetic model ($f(\alpha) = 2\alpha^{1/2}$) gives the value of E_a which is consistent with the value obtained from the isothermal conditions. The critical temperature (T_c) of decomposition process was determined. The resulting value of T_c was in fairly good agreement with the starting temperature of thermal decomposition of silver oxide (Ag_2O). The thermodynamic functions of decomposition process are calculated by the activated complex theory and showed that the silver–oxygen bond secession can be interpreted as a "slow" stage of the decomposition process.

1. Introduction

Nanotechnology is an important field of modern research dealing with design, synthesis, and manipulation of particles structure ranging from approximately 1 to 100 nm. Tremendous growth in this emerging technology has opened novel fundamental and applied frontiers, including the synthesis of nanoscale materials and exploration or utilization of their exotic physicochemical and optoelectronic properties. Nanotechnology is rapidly gaining importance in a number of areas such as health care, cosmetics, food and feed, environmental health, mechanics, optics, biomedical sciences, chemical industries, electronics, space industries, drug-gene delivery, energy science, optoelectronics, catalysis, reprography, single electron transistors, light emitters, nonlinear optical devices, and photo-electrochemical applications [1–7].

Silver, in its native form, was discovered as early as 3000 BC. Owing to its unique properties such as strength, malleability, ductility, thermal and electrical conductivity, and microbial properties – silver has found wide applications in industry and medicine. The emergence of silver nanoparticles and their unique properties has taken the nanotechnology industry by a storm. According to the market research conducted by Bourne Research, silver nanoparticles are emerging as one of the fastest growing product categories in the nanotechnology industry. Silver due to its excellent biocompatibility and antibacterial property raise considerable interest as nanoparticles for biomedical applications [8].

Important applications for silver particles can be found in the catalyst and the electronic industry [9–11]. For example, the production of formaldehyde and ethylene oxide can benefit from the use of silver comprising nanoscale catalysts. Silver dissociates molecular oxygen from the air and weakly holds the separated oxygen atoms until an alkene, such as ethylene, reacts with them to form respective alkene oxide. Silver comprising nanoparticles prepared by the ultrasonic spray pyrolysis (USP) [12] method offer the potential to reach a number of surprising and unique advantages.

* Corresponding author. Tel.: +381 11 2187 133; fax: +381 11 2187 133.
E-mail address: bojanjan@ffh.bg.ac.rs (B. Janković).

http://dx.doi.org/10.1016/j.cep.2014.06.002
0255-2701/

Especially, the unique interaction between silver in nanoparticle form and oxygen is high interest for the catalytic industry. The USP is an innovative and powerful tool for the synthesis of particles with controlled and uniform particle size because of the easy control of the powder morphology and the excellent availability of cheap precursors and the low operation costs [13–16].

Chemical bonds between the silver nanoparticles and the organic shell function as a passivation layer that prevents the self-cohesion of the nanoparticles. The fine Ag-particles (average particle size of 100 nm) were used by Ide et al. [10] as a reference material to consider the effect of particle size on bond ability. By reducing the metal particle size, the surface energy and the vapor pressure increase proportionately with the inverse of the particle radius, and this strongly influence the sintering of particles and the bond abilities to copper. Solid, spherical, micron-sized silver particles were produced from a silver nitrate solution. Pluym et al. [9] show effects of the reaction temperature, carrier gas type, solution concentration, and the aerosol droplet size on the characteristics of the resultant silver particles. Pure, dense un-agglomerated particles were obtained using an ultrasonic generator at and the above 600 °C, under nitrogen as the carrier gas, and above 900 °C using air as the carrier gas. Solid particle formation at temperatures below the melting point of silver (962 °C) was attributed to sufficiently long residence times, which allowed the aerosol-phase densification of the porous silver particles resulting from the reaction of the precursor. As the precursor solution concentration was increased from 0.5 to 4.0 M, the particle size increased from 1.03 to 1.68 μm. In addition, when the particles are reduced in size to less than 100 nm, their characteristics are different from those of the bulk state [11]. For example, the melting point and the sintering temperature are detectably lower.

The USP has been successfully used by the authors for the preparation of nano-sized silver particles from commercial silver nitrate [17]. The results of the thermodynamic analysis of the decomposition of commercial silver nitrate used as precursors for the formation of silver powders by the USP method were revealed, that the equilibrium in presence of *hydrogen* is possible at room temperature, in difference to 400 °C in the absence of hydrogen. The increase of the hydrogen reduction temperature from 150 °C to 1000 °C increases the amount of spherical, dense particles in the Ag-powder structure but there is no influence on the purity of the obtained powder of silver [17]. The thermo-analytical (TA) measurements of commercial silver nitrate decomposition process in an inert (*nitrogen*) atmosphere under non-isothermal conditions have been shown that the process proceeds through the chemical rate controlled reactions (depending to the reaction temperature), with the average apparent activation energy of E_a = 137.0 kJ mol^{-1}, for the heating rates between 5 and 40 °C min^{-1} [18]. The thermochemical investigations have shown that in a *nitrogen* atmosphere, the silver formation starts at 400 °C, while in a *hydrogen* atmosphere, the actual hydrogen reduction of silver nitrate is possible in the temperature range between 20 °C and 1000 °C [17,18]. The X-ray diffraction analysis and SEM results were shown the presence of the spherical silver particles in the particle size range between 7 and 930 nm, with an average particle size ranged from 136 to 241 nm. The SMPS – online data (168 nm) showed acceptable agreement with theoretical calculations as well as with SEM analyses [18]. It has been shown on the basis of the obtained results [18], that an increase in concentration of silver nitrate leads to larger particles size of silver.

The main objective of this paper is to examine the kinetic and thermodynamic behaviors of a commercial silver nitrate when it is subjected to thermal decomposition under non-isothermal conditions in an inert atmosphere of argon. An important point in this paper is given to the mechanistic interpretation of the process and comparing the results of the current kinetic analysis, with the results of kinetic tests obtained for the same system, but in different atmospheres such as hydrogen and nitrogen. Investigations of this type are necessary in order to compare the results of the kinetic behavior of the precursors for the USP application, in the different reaction atmospheres, because, we believe that the mechanism of the decomposition process developments, largely depends on "the nature of the reaction medium" and this fact is very important in industrial applications. Namely, the reaction atmosphere can significantly contribute to the regulation of temperature range in which the particles of metallic silver are formed, as well as their overall geometrical shape and dimensions.

2. Experimental

2.1. Material

Silver nitrate, $AgNO_3$ (Merck, Darmstadt, Germany, purity 99.999%), in the form of salt agglomerations was submitted to experimental measurements. This material was used as the precursor for the preparation of silver powders by the ultrasonic spray pyrolysis [18].

2.2. Thermal measurements

The decomposition behavior of silver nitrate was investigated using the simultaneous TGA-DTA equipment Netzsch STA 409 CD Thermal Analyzer (Netzsch-Gerätebau GmbH, Wittelsbacherstraße 42, 95100 Selb, Germany), with experimental temperature range from −160 °C up to 2000 °C (with different types of furnaces), and with sensitivity of max. 1 digit/1.25 μg. Operating system has Software features (the graphic interface MS Windows^{TM}), with a graphic presentation of results during measurements. The thermal measurements were conducted under an argon (Ar) atmosphere (with a gas flow rate of φ = 150 mL min^{-1}), in a temperature range between 25 °C and 1000 °C, with α-Al_2O_3 crucibles. Samples in powder form with a mass of approximately $m \approx 10.586$ mg (as the average mass value), were used in measuring in a linear heating modes, at the heating rates of β = 5, 10, 20 and 40 °C min^{-1}. All TGA (thermogravimetric analysis) and DTA (differential thermal analysis) results of the investigated decomposition process are compounded by the data export options (as ASCII file).

3. Theoretical background

3.1. Kinetic analysis

Knowledge of kinetic parameters, such as the reaction rate and the apparent activation energy, is one of the keys to determine the reaction mechanisms in solid phases. When changes in the mechanisms are observed, this can lead to a unique characteristic and hence a better knowledge of the materials. Besides this, there are also more practical reasons to know the reaction rates and their temperature dependence. The industry needs measurements of those parameters for the accurate design of installations and treatment conditions, because augmentation of temperature or elongation of reaction time means more costs. Using an appropriate mathematical expression, the thermo-analytical (TA) experiments can be applied for the modeling of industrial thermal processes. The results of the kinetic investigation of thermo-analytical reactions in the solid state can also be applied to problems as useful lifetime of investigated material, oxidation–reduction material properties, thermal stability and quality control. In order to obtain the quality values of kinetic parameters (the apparent activation energy (E_a), the pre-exponential factor (A), including and the analytical form of the reaction mechanism function in differential or integral

form ($f(\alpha)$ or $g(\alpha)$ (where α represents the extent of conversion)) – the kinetic 'triplet' [19]) from thermal analysis data, the combined use of the simultaneous thermogravimetric and differential thermal analysis (TGA–DTA) was advocated.

The mathematical methods to process the thermo-analytical data can be divided into the *model-fitting* and *model-free* (*isoconversional*) methods [20,21]. The model fitting approach has the advantage that only one TA measurement is needed. On the other hand, this approach suffers from an inability to determine the reaction model function uniquely [20,22]. In spite of this unreliability, it is a quick method to become a first indication of possible values for the kinetic parameters. The alternative model-free methodology is based on the *isoconversional* principle. The use of these methods helps to avoid the problems that originate from the ambiguous evaluation of the reaction model. The model-free methodology allows the determination of the dependence of the apparent activation energy on the extent of conversion and permits reliable mechanistic conclusions to be drawn [20,22]. A negative aspect is the need for at least three TA experiments what makes it more time consuming.

In the presented study, we combined the model-fitting and model free approaches, with the use of different kinetic evaluations, in order to determine reliable kinetic mechanism of the non-isothermal decomposition process of silver nitrate as precursors for the USP procedure. Kinetic analysis was given on the basis of ICTAC Kinetics Committee recommendations for performing kinetic computations [23].

3.1.1. Model-free (isoconversional) kinetic approach

The kinetic analysis of solid-state thermal decomposition is usually given by Eq. (1) [20]:

$$\frac{d\alpha}{dt} = A \cdot \exp\left(-\frac{E_a}{RT}\right) \cdot f(\alpha) \tag{1}$$

where $d\alpha/dt$ is the rate of decomposition, α is the extent of conversion (the degree of decomposition) which is defined as $\alpha = (m_0 - m_t)/(m_0 - m_f)$, where m_0 and m_f are the initial and final masses of the sample under decomposition, respectively, and m_t is the mass of the sample at time t (or temperature, T); A is the pre-exponential factor [min^{-1}], E_a is the apparent activation energy [$\mathrm{kJ\,mol}^{-1}$], R is the gas constant 8.314 [$\mathrm{J\,mol}^{-1}\,\mathrm{K}^{-1}$], T is the absolute temperature [K], and $f(\alpha)$ is a mathematical model function of the kinetics, which depends on the reaction type and reaction mechanism.

Taking into account the heating rate $\beta = dT/dt$ under the non-isothermal condition, the kinetic analysis of solid-state thermal decomposition can be described by Eq. (2), in the following form:

$$\frac{d\alpha}{dt} \equiv \beta \cdot \frac{d\alpha}{dT} = A \cdot \exp\left(-\frac{E_a}{RT}\right) \cdot f(\alpha), \tag{2}$$

where the integral form of Eq. (2) can be presented as:

$$g(\alpha) = \int_0^{\alpha} \frac{1}{f(\alpha)} d\alpha = \frac{A}{\beta} \int_0^{T} \exp\left(-\frac{E_a}{RT}\right) dT = \frac{A}{\beta} \cdot I(E_a, T). \tag{3}$$

In Eq. (3), $g(\alpha)$ is the integral form of the model function that does not depend on the heating rate used. Integration of Eq. (2) involves solving the temperature integral in Eq. (3). Since the integral $I(E_a,T)$ in Eq. (3) does not have an analytical solution it can be solved using either approximations or numerical integration. One of the simplest approximations by Doyle's [24] gives rise to the following Eq. (4), which is used in frequency applied method, known as the Ozawa–Flynn–Wall (OFW) isoconversional method [25,26]:

$$\ln\ \beta = \ln\left[\frac{AE_a}{Rg(\alpha)}\right] - 5.331 - 1.052 \cdot \frac{E_a}{RT} \tag{4}$$

According to this method, the apparent activation energy (E_a) is calculated at given values of conversion (α) from a plot of $\ln \beta$ versus $1/T$. It is important that this method provides estimation of E_a at every selected and constant α value ($\alpha = const.$) without knowledge of the specific reaction function. The OFW method assumes that E_a is constant, thus a systematic error in the estimation of E_a should be expected, whenever E_a varies with α [27]. If the results show a change in E_a during the progress of reaction, the variable separation used in this method becomes invalid.

Use of another asymptotic approximation for the temperature integral yielded the following equation, known as the Kissinger–Akahira–Sunose (KAS) method [28,29]:

$$\ln\left(\frac{\beta}{T^2}\right) = \ln\left[\frac{AR}{E_a g(\alpha)}\right] - \frac{E_a}{RT} \tag{5}$$

Evaluation of the apparent activation energy is achieved from the plot of $\ln(\beta/T^2)$ versus $1/T$ at constant values of α ($\alpha = const.$) and the heating rate, β.

The next isoconversional integral method was proposed by Tang (T) [30], with a more precise formula for the temperature integral which is as follows:

$$\ln\left(\frac{\beta}{T^{1.894661}}\right) = \ln\left[\frac{AE_a}{Rg(\alpha)}\right] + 3.635 - 1.894661\ \ln E_a - 1.00145033 \cdot \frac{E_a}{RT} \tag{6}$$

The apparent activation energy (E_a) at a particular value of α can be estimated by plotting $\ln(\beta/T^{1.894661})$ versus $1/T$ across different heating rate values. The pre-exponential factor (A), as in the case of the two previous *model-free* methods, can be calculated only when we know the analytical form of the function $g(\alpha)$.

The isoconversional differential method suggested by Friedman (FR) [31], shown in Eq. (7) is obtained by simple rearrangement of Eq. (2):

$$\ln\left(\frac{d\alpha}{dt}\right) \equiv \ln\left[\beta\left(\frac{d\alpha}{dT}\right)\right] = \ln[A \cdot f(\alpha)] - \frac{E_a}{RT}. \tag{7}$$

Eq. (7) provides E_a value by the slope of the graph of $\ln(d\alpha/dt)$ versus $1/T$ at each specific extent of conversion (α). Although no approximations are introduced in Eq. (7), the Friedman method is affected by significant numerical instability and noise interference because it employs instantaneous rate values and uses the differential term $d\alpha/dt$ in the numerical calculations. Therefore, the Vyazovkin (V) method was developed to eliminate the systematic error in E_a, when it varies with α [32].

Vyazovkin [32] has developed an advanced non-linear procedure that performs integrations over small conversion intervals, $\Delta\alpha \approx 0.01$, where E_a is considered constant. Then, for a series of n experiments at the different heating rates, E_a is determined for each interval as the value that minimizes the function given by Eq. (9). Systematic errors associated with major integrations are then minimized by this method [32], and can be represented by the following set of equations:

$$J[E_{a\alpha}, T(t_\alpha)] = \int_{t_\alpha - \Delta\alpha}^{t_\alpha} \exp\left(-\frac{E_{a\alpha}}{RT(t)}\right) dt, \tag{8}$$

and

$$\sum_{i=1}^{n} \sum_{j \neq i}^{n} \frac{J\,[E_{a\alpha}, T_i(t_\alpha)]}{J\,[E_{a\alpha}, T_j(t_\alpha)]} = \min., \tag{9}$$

where indexes i and j in Eq. (9) denote different heating rates, while n is the total number of the heating rates, and J represents the temperature integral (Eq. (8)). Eq. (9) is formulated such that it is

possible for the integration in Eq. (8) to be performed over small steps of $\Delta\alpha$. In the current study, we have used step of $\Delta\alpha = 0.01$, in strictly characterized conversion frontiers, from 5% to 95% of total decomposition. The integral presented by Eq. (8) can be evaluated numerically, using the trapezoidal rule, for a set of experimental heating programs. This approach severely reduces the systematic error observed in other *integral* methods which are essentially integrated using $\Delta\alpha = \alpha$.

3.1.2. Model-fitting kinetic approach

One of the best-known method's that belongs to the group of the model-fitting methods is precisely the Coats and Redfern (CR) [33] kinetic procedure, for the estimation of the kinetic parameters. This method utilizes the asymptotic series expansion for approximating the temperature integral giving

$$\ln\left[\frac{g(\alpha)}{T^2}\right] = \ln\left[\frac{AR}{\beta E_a}\left(1 - \frac{2R}{E_a}\bar{T}\right)\right] - \frac{E_a}{RT} \tag{10}$$

where $\bar{T}$ is the mean experimental temperature. Since E_a is in kJ mol^{-1}, then there is usually present inequality $2R\bar{T}/E_a \ll 1$ [34], Eq. (10) is reduced to Eq. (11) as:

$$\ln\left[\frac{g(\alpha)}{T^2}\right] = \ln\left(\frac{AR}{\beta E_a}\right) - \frac{E_a}{RT} \tag{11}$$

Plotting the left-hand side of Eq. (11), which includes the reaction model function $g(\alpha)$ versus $1/T$ fives E_a and A from the slope and the intercept, respectively. This method requires only the relative mass of the sample, from which $g(\alpha)$ is determined as a function of decomposition temperature to determine the apparent activation energy of the process. Generally, the model that gives the best linear regression fit is selected as the chosen model. The various analytical forms of model function $g(\alpha)$ were derived on the basis of physical and geometrical considerations, and they exist in the literature [19,20,23,35,37]. It should be noted that it has been shown [35,36], that the CR method in the case of the investigated processes which show the simple reaction mechanisms, the plot of $\ln[g(\alpha)/T^2]$ versus $1/T$ will be linear for many reaction kinetic models and the reaction mechanism can not be truly recognized. On the other hand, for the processes having very complex mechanisms (with multiple reaction stages), the plot of $\ln[g(\alpha)/T^2]$ versus $1/T$ will not be linear and the CR method is *not* valid for kinetic analysis to find the appropriate kinetic model and the reliable kinetic parameters.

The kinetic composite methods presuppose one single set of the kinetic parameters for all conversions and the heating rates. In this way all the experimental data can be superimposed in one single master curve.

The composite integral method (I) [38,39] is based on the Coats and Redfern (CR) equation, which is rewritten as follows:

$$\ln\left[\beta \cdot \frac{g(\alpha)}{T^2}\right] = \ln\left(\frac{AR}{E_a}\right) - \frac{E_a}{RT} \tag{12}$$

For each form of considered $g(\alpha)$ function, the curve the curve $\ln[\beta \cdot g(\alpha)/T^2]$ versus $1/T$ was plotted for the experimental data obtained at the different heating rates. In this case, then we choose the kinetic model for which the data falls in a single master straight line and which gives the best linear regression coefficient. The single set of kinetic parameters (A and E_a), can be obtained from the intercept and the slope of the straight line.

The differential version of this method (the composite differential method (I)) [40] is based directly on Eq. (2):

$$\ln\left[\frac{(d\alpha/dt)}{f(\alpha)}\right] = \ln(A) - \frac{E_a}{RT} \tag{13}$$

For a given reaction model function ($f(\alpha)$) and heating rate, the linear plot of $\ln[(d\alpha/dt)/f(\alpha)]$ versus $1/T$, allow us to get the single set of kinetic parameters (A and E_a) from the intercept and the slope of the straight line. The data for different heating rates must be grouped together in a single relation, from which, the single set of kinetic parameters is calculated.

3.1.3. The critical temperature (T_c) for thermal decomposition process

Based on the multiple non-isothermal DTA curves obtained at four different heating rates (5, 10, 20 and 40 °C min^{-1}), the values of the onset (initial) (T_i), and the peak temperature (T_p) can be estimated for considered decomposition process. On the basis of the functional dependence between T_i and β, and for the zero approximation of the heating rate (when $\beta \to 0$ °C min^{-1}), the critical temperature (T_c) for investigated decomposition process (T_c represents the important thermal stability parameter, which can be defined as the lowest temperature to which the investigated material may be heated without undergoing thermal decomposition) can be calculated from the following equation [41,42]:

$$T_c = \frac{E_a^{OFW} - \sqrt{(E_a^{OFW})^2 - 4 \cdot E_a^{OFW} R \cdot T_i^{\beta \to 0}}}{2 \cdot R} \tag{14}$$

where E_a^{OFW} is the value of the apparent activation energy calculated by OFW method, $T_i^{\beta \to 0}$ represents the value of the onset (initial) temperature for $\beta \to 0$ °C min^{-1}, and R is the gas constant. The value of $T_i^{\beta \to 0}$ can be estimated from relation between T_i and β corresponding to $\beta \to 0$ °C min^{-1}. Therefore, the determination of T_c is a good way to gain thermal stability and determining the threshold for temperature-stress in the case of tested system.

The Arrhenius equation can be expressed with E_a^{OFW} (the average value of E_a^{OFW}) and $\ln A_{OFW}$ (the average value of $\ln A_{OFW}$ from Eq. (4), and for determined analytical form of the function $g(\alpha)$) as follows:

$$\ln(k)_{critical} = \ln A_{OFW} - \frac{E_a^{OFW}}{RT_c} \tag{15}$$

The above equation can be used to estimate the rate constant at the critical temperature ($(k)_{critical}$).

3.1.4. Determination of the reaction mechanism

3.1.4.1. The master plot method. According to this method [43,44], the master plots can be drawn based on either the integral or the differential form of the kinetic equation describing decomposition by using the concept of the generalized time, θ. From the integral kinetic equation the following equation can be obtained using a reference point at $\alpha = 0.50$:

$$\frac{g(\alpha)}{g(0.50)} = \frac{\theta}{\theta_{0.50}}. \tag{16}$$

During non-isothermal experiments at a linear heating rate, the right-hand side of Eq. (16) can be calculated by following expression:

$$\frac{\theta}{\theta_{0.50}} = \frac{p(x)}{p(x_{0.50})}, \tag{17}$$

where for the function $p(x)$ ($x = E_a/RT$ is the reduced apparent activation energy), the fourth rational approximation of Senum and Yang [45,46] corrected by Flynn was used in our calculation procedures, and which allows an accuracy of better than 10^{-5}% [43].

3.1.4.2. The invariant kinetic parameters (IKP) method. The method of invariant kinetic parameters (IKP) [47] makes use of the so-called "compensation effect" that is observed when a *model-fitting* method is applied to a single-heating rate run. The IKP method allows us to perform the "true" kinetic model [48]. Accordingly, sets of $\ln A$ and E_a parameters are obtained at different heating rates β, using the Coats and Redfern (CR) method (Eq. (11)). Algebraic expressions for $g(\alpha)$ functions, for the most frequently used

mechanisms are known in the literature [19,20,23,35,37]. For each theoretical kinetic model, $g(\alpha)$, and at each heating rate, β, from the slope and the intercept of the plots $\ln[g(\alpha)/T^2]$ versus $1/T$, the kinetic parameters E_a and $\ln A$ can be evaluated.

If the compensation effect between $\ln A$ and E_a exists, then by plotting $\ln A$ against E_a, the straight lines should be obtained for each heating rate, according to

$$\ln A = a_v^* + b_v^* \cdot E_a \tag{18}$$

These lines should intersect in a point that corresponds to the "true" values of E_a and A for the "true" kinetic model, which were called by Lesnikovich and Levchik the invariant kinetic parameters, $E_{a,inv}$ and A_{inv} [47].

Due to the fact that certain variations of the experimental conditions determine regions of intersection, the intersection is only approximate. Therefore, in order to eliminate the influence of experimental conditions on the determination of A_{inv} and $E_{a,inv}$, they are determined from the slope and intersect of the so-called supercorrelation relation in the form:

$$a_v^* = \ln A_{inv} - b_v^* \cdot E_{a,inv}. \tag{19}$$

It should be noted here that the IKP method can be used only if E_a does not depend on α (i.e. whether the process can be described as the single-step kinetics [23]). This can be checked by application of isoconversional methods and making sure that $E_{a,\alpha}$ does not vary significantly with α. It should also be noted that when when choosing the reaction (kinetic) models for calculation of $\ln A$ and E_a (Eq. (18)), it is advisable to pick a set of models that yields a wide range of the $\ln A$ and E_a values. The wider the range, the smaller the error in determining the parameters of the compensation effect, a_v^* and b_v^* [23]. It is important to use a wider range of the heating rates to secure smaller errors in estimating of $\ln A_{inv}$ and $E_{a,inv}$ [23].

Furthermore, the IKP method can be used for the numerical evaluation of the $f_{inv}(\alpha)$ function by introducing the values of the invariant kinetic parameters, $E_{a,inv}$ and A_{inv}, into the following equation of the form:

$$f_{inv}(\alpha) = \frac{(d\alpha/dt)}{A_{inv} \cdot \exp(-(E_{a,inv}/RT))} \tag{20}$$

where $f_{inv}(\alpha)$ represents the invariant kinetic function for investigated decomposition process.

The accurate determination of the reaction model and the pre-exponential factor can be accomplished by using the applied compensation effect (Eq. (18)). For this purpose, the A and E_a values are used to determine the a_v^* and b_v^* parameters of the compensation effect. Then, substitution of the *model-free* apparent activation energy ($E_{a,mf}$) into Eq. (18) gives a model-free estimate for the pre-exponential factor, A_{mf}, in the form:

$$\ln A_{mf} = a_v^* + b_v^* \cdot E_{a,mf} \tag{21}$$

The determination of the reaction model requires that a variation of $E_{a,\alpha}$ with α to be negligible so that the $E_{a,\alpha}$ dependence can be replaced with a single average value, $E_{a,mf}$. Once both, $E_{a,mf}$ and A_{mf} have been determined, one can *numerically reconstruct* the reaction model in either integral or the differential form. The *integral* form can be reconstructed by substituting the values of $E_{a,mf}$ and A_{mf} into Eq. (3) that takes the following form [23]:

$$g(\alpha) = \frac{A_{mf}}{\beta} \int_0^{T_\alpha} \exp\left(-\frac{E_{a,mf}}{RT}\right) dT. \tag{22}$$

Eq. (22) allows us to obtain a set of numerical values of $g(\alpha)$ corresponding to different values of α. The resulting numerical values of $g(\alpha)$ should not demonstrate any significant variation with β giving rise to a single dependence of $g(\alpha)$ on α. The analytical form of reaction model can then be established by plotting the numerical values of $g(\alpha)$ against the theoretical dependencies, obtained from the $g(\alpha)$ equations representing the reaction models, and finding best matching with theoretical dependence.

The corresponding *rate constant* for investigated decomposition process can be found from the *modified* equation of the compensation effect, using the values of the peak temperature (T_p), in the analytical form as:

$$\ln A = \ln\left[\frac{E_a \cdot (\beta)^p_{const.}}{R \cdot T_p^2}\right] + \frac{E_a}{RT_p} \tag{23}$$

where the kinetic parameters $\ln A$ (left-hand side of Eq. (23)) and E_a (in square brackets in the right-hand side of Eq. (23)) are associated with some special *model-free* (*peak*) *isoconversional method*, such as the Kissinger method [28] (in other words, it is considered that these values are derived primarily from the Kissinger method), while $(\beta)^p_{const.}$, represents the corresponding value of the heating rate, where we look at the value of T_p. The term $E_a \cdot (\beta)^p_{const.}/R \cdot T_p^2$ is the *rate constant* [min^{-1}] of the process observed at each T_p.

3.1.5. Determination of the pre-exponential factor using values of α_p and T_p

The α_p values (α_p represents the conversion value that had been achieved in T_p) can provide some extra help in identifying appropriate reaction models for experimental data [44]. Once the reaction model has been identified, the pre-exponential factor (A) is determined from the following equation [23]:

$$A = -\frac{\beta \cdot E_a}{R \cdot T_p^2 f'(\alpha_p)} \exp\left(\frac{E_a}{RT_p}\right) \tag{24}$$

where E_a represents the average value of the apparent activation energy, calculated by the *model-free* (isoconversional) approach (Section 3.1.1), while the subscript p denotes the values attached to the maximum of the differential kinetic curve obtained at a given heating rate, β; $f'(\alpha)$ represents the corresponding value of $df(\alpha)/d\alpha$ function in the singularity corresponding to the α_p value.

3.1.6. The kinetic predictions of investigated process

Kinetic prediction procedure represents the most important practical application of kinetic analysis. The purpose of kinetic analysis is to parameterize the process rate in terms of such variables as the temperature, the extent of conversion and sometimes pressure. The parameterization is accomplished by evaluating parameters of the equations that describe the effect of the variables on the process rate [23]. From such analysis, the important parameter can be evaluated – this is so-called the *lifetime*. The lifetime of a material is the time after which the material loses its properties to such extent that it cannot fulfill efficiently the function for which it was created [23,49]. All materials change their properties to some extent when exposed to heat. Usually it is necessary to define some limiting extent of decay beyond which the material becomes unusable, e.g., 5% decay relative to the initial value that would be equivalent to reaching $\alpha = 0.05$, and in this case we mark the lifetime as $t_{0.05}$ or $t_{5\%}$.

In the case of a single-step process taking place under isothermal conditions (the constant operating temperature, T_o), the time to reach a given conversion, can be expressed through the following equation:

$$t_\alpha = \frac{g(\alpha)}{A \exp(-(E_a/RT_o))} \tag{25}$$

Eq. (25) can be used to predict the lifetime of investigated material under isothermal conditions at the operating temperature T_o. The prediction requires knowledge of the kinetic triplet for the

considered process. The kinetic triplet can be determined from either isothermal or non-isothermal experiments.

In the case of "model-free predictions", we have the elimination of the kinetic model $g(\alpha)$ in Eq. (25). The "model-free predictions" are not limited to a given form of $g(\alpha)$ function, and are applicable to to the processes for which $E_{a,\alpha}$ varies with α, then these predictions generally produce more reliable estimates for the lifetime, $t_{\alpha.}$ In the case of "model-free prediction", the following equations apply:

$$t_\alpha = \frac{\int_0^{T_\alpha} \exp(-(E_{a,\alpha}/RT))dT}{\beta \cdot \exp(-(E_{a,\alpha}/RT_o))} \tag{26}$$

and

$$t_\alpha = \frac{J\left\lfloor E_{a,\alpha}, T(t_\alpha)\right\rfloor}{\exp(-(E_{a,\alpha}/RT_o))}. \tag{26a}$$

where the last equation is adaptable for the arbitrary heating programs [23].

As one of the important factors that affect the accuracy and reliability of the kinetic prediction is the experimental temperature range. In this sense, the experimental temperature range should be brought as close as possible to the temperature range of predictions. An important fact should be noted, that prior to the commission of predictions, it should be checked whether the experimentally evaluated kinetic parameters *can be used* to reconstruct accurately the experimental data that were used to evaluate the mentioned parameters.

3.2. Thermodynamic analysis

From the activated complex theory (transition state) of Eyring [50–53], the following general equation may be written:

$$A = \left(\frac{e\chi k_B T_p}{h}\right) \cdot \exp\left(\frac{\Delta S^{\neq\circ}}{R}\right) \tag{27}$$

where A is the pre-exponential factor (where A can be obtained from Eq. (24)), e is the Neper number ($e = 2.7183$), χ is the transition factor, which is unity for monomolecular reactions, k_B is the Boltzmann constant ($k_B = 1.38065 \times 10^{-23}\,\mathrm{J\,K^{-1}}$), h is the Planck constant ($h = 6.62607 \times 10^{-34}\,\mathrm{J\,s^{-1}}$), and T_p represents the peak temperature from the DTA curve. The change of the entropy may be calculated according to the following formula:

$$\Delta S^{\neq\circ} = R \cdot \ln\left(\frac{A \cdot h}{e \cdot \chi \cdot k_B \cdot T_p}\right). \tag{28}$$

Since

$$\Delta H^{\#\circ} = E_a^* - R \cdot T_p \tag{29}$$

when E_a^* represents the apparent activation energy calculated by the *model-free* (isoconversional) method. The changes of the enthalpy ($\Delta H^{\neq\circ}$) and the Gibbs free energy ($\Delta G^{\neq\circ}$) for the activated complex formation from the reagent can be calculated using the well-known thermodynamic equation:

$$\Delta G^{\neq\circ} = \Delta H^{\neq\circ} - T_p \cdot \Delta S^{\neq\circ} \tag{30}$$

The heat of activation ($\Delta H^{\neq\circ}$), the entropy of activation ($\Delta S^{\neq\circ}$), and the free energy of activation of the decomposition process ($\Delta G^{\neq\circ}$) were calculated at $T = T_p$, where T_p is very important thermal analysis parameter.

In addition, the thermodynamic parameters ($\Delta H^{\neq\circ}$, $\Delta S^{\neq\circ}$ and $\Delta G^{\neq\circ}$) can be calculated from the equation, which includes the variation of the thermodynamic equilibrium constant (K_o), in the form as:

$$\ln K_o = \frac{\Delta S^{\neq\circ}}{R} - \frac{\Delta H^{\neq\circ}}{RT}, \tag{31}$$

and

$$\Delta G^{\neq\circ} = -RT \ln K_o \tag{32}$$

where K_o^T at considered particular reaction temperature T can generally be expressed as:

$$K_o^T = \exp\left(-\frac{\Delta G^{\neq\circ,T}}{RT}\right), \tag{33}$$

and where $\Delta H^{\neq\circ}$, $\Delta S^{\neq\circ}$ and $\Delta G^{\neq\circ}$ have dimensions of $\mathrm{kJ\,mol^{-1}}$, $\mathrm{kJ\,mol^{-1}\,K^{-1}}$ and $\mathrm{kJ\,mol^{-1}}$, respectively. The values of $\Delta H^{\neq\circ}$ and $\Delta S^{\neq\circ}$ can be obtained from the slope and intercept of the plot of $\ln K_o$ against $(1/T)$ (Eq. (31)). The temperatures T in Eq. (31) represent selected operating temperatures that are characteristic for a given equilibrium constants accompanying the decomposition process under study.

4. Results and discussion

4.1. Thermal characterization

Fig. 1 shows TGA–DTA curves recorded at $\beta = 20\,^\circ\mathrm{C\,min^{-1}}$, for non-isothermal decomposition process of a commercial silver nitrate in an argon (Ar) atmosphere. All thermo-analytical (TA) curves are presented up to a temperature of 700 °C, because the above mentioned temperature any changes are not observed (the complete saturation was observed in all curves).

The investigated sample shows a very small mass loss (which is exactly 0.19%) in the temperature range from 30 to 200 °C (TGA – Fig. 1). From Fig. 1 we can see that the first, rather broader endothermic peak located at 160 °C, can be attributed to the phase transition (II → I transition) in $AgNO_3$, which is usually accompanied by changes in crystallographic, thermodynamic, electrical and optical properties [54–57]. In addition, we can see that there is an overlapping of the first endothermic peak with the following endothermic (less intense) peak, located at approximately 210 °C (Fig. 1). The aforementioned peak can be attributed to the melting process of $AgNO_3$ [58,59]. The peak marked by "I" in Fig. 1 actually corresponds to the completion of melting process.

It can be seen from Fig. 1 that after the above mentioned transformations of $AgNO_3$, we can notice the presence of endothermic

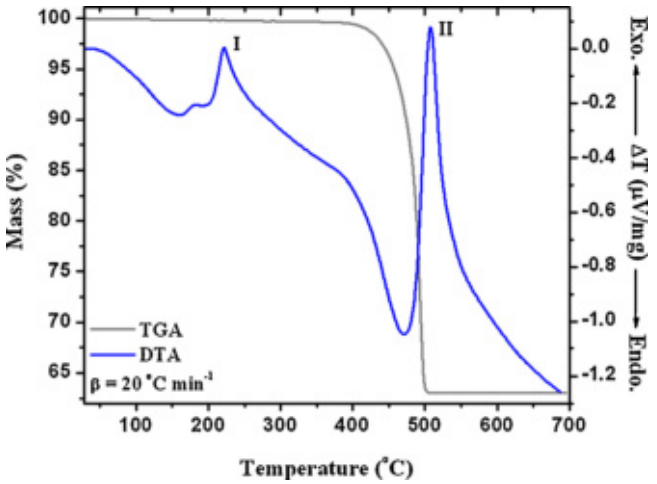

Fig. 1. TGA–DTA curves recorded at $\beta = 20\,^\circ\mathrm{C\,min^{-1}}$, for non-isothermal decomposition process of a commercial silver nitrate in an argon (Ar) atmosphere.

Table 1
The values of characteristic peak temperatures (T_p) attached with a *main* decomposition process, together with values of α_p (conversions at T_p) and the residual mass losses (Δm%), at the different heating rates (β = 5, 10, 20 and 40 °C min^{-1}), for the non-isothermal decomposition of commercial silver nitrate in an argon (Ar) atmosphere.

β (°C min^{-1})	T_p (°C) [a]	α_p	Δm (%) [b]
5	454.70	0.697	63.20
10	480.25	0.686	63.18
20	491.92	0.661	63.00
40	519.69	0.637	62.75
Average	486.64	0.670	63.03

[a] T_p from DTG curves.
[b] Δm from TG curves.

effect (after the temperature of 405 °C), which is characterized by the peak located at 468 °C. It should be noted that the boiling point of $AgNO_3$ is 444 °C and a boiling is immediately followed by the decomposition process. On the other hand, the peak located at 508 °C (marked by "II" in Fig. 1) is situated at a temperature higher than the temperature at which the decomposition of $AgNO_3$ is finished. The change of DTA signals around temperature of 500 °C may belong to the change of heat capacity [60]. The residual mass loss of the sample, at a given heating rate (Fig. 1), after the formation of the final product, is exactly 63.00%.

It should be noted that the appearance of the endothermic process in the "central" temperature region (Fig. 1) could be attributed to the appearance of "*intermediary compounds*" (probably metal oxide), and the consumption of additional energy cleaving the covalent bonds present in the metal oxide. However, this view on the given decomposition process, in this phase of testing, it would be too speculative, since the present system (depending on the reaction atmosphere (whether in terms of inert gases such as N_2, Ar or the oxidation protection (oxygen)) and the experimental parameters (such as heating rate and partial pressures of gases released during the process)) may exhibit different reaction pathways, given with an previous research by Makela et al. [61]. Therefore, it is necessary to perform a detailed kinetic analysis, including a combination of various kinetic procedures, in order to consider a general and practically applicable mechanistic picture of the entire process.

Table 1 shows the values of characteristic peak temperatures (T_p) attached with a *main* decomposition process (Fig. 1), together with values of α_p (conversions at T_p) and the residual mass losses (Δm (%)), at the different heating rates (5, 10, 20 and 40 °C min^{-1}). The values of T_p in Table 1 were obtained from the experimental DTG curves at the different heating rates, and these curves are presented in Fig. 2. We can see that all DTG peaks (Fig. 2) are located in the temperature range of ΔT = 400–550 °C at all considered heating rates (5, 10, 20 and 40 °C min^{-1}).

From Table 1 we can see that with an increasing of heating rate (β), the values of T_p shifted to a higher decomposition temperature zone. In addition, the values of α_p vary in the range from 0.637 (40 °C min^{-1}) to 0.697 (5 °C min^{-1}), with average value which amounts α_p (*av.*) = 0.670. On the other hand, the residual mass loss (Δm (%)) of the investigated samples varies very little with the heating rate, with the characteristic average value of Δm (*av.*) = 63.03% (Table 1). All identified T_p values observed on the DTG curves are shifted to higher temperatures with increasing the heating rate, indicating a typical thermal-activated process. It should be noted that the value of α_p can be used for preliminary identification of the reaction mechanism, based on the theoretical ranges in which the values of α_p vary with the heating rate [62]. The values of α_p shown in Table 1, may includes the various reaction models, such as the power law models with nucleation type of reactivity (Avrami-Erofeev), through the diffusion (D*n*) and geometrical models (the contracting type of kinetic models (R*n*)) [62,63]. However, with this

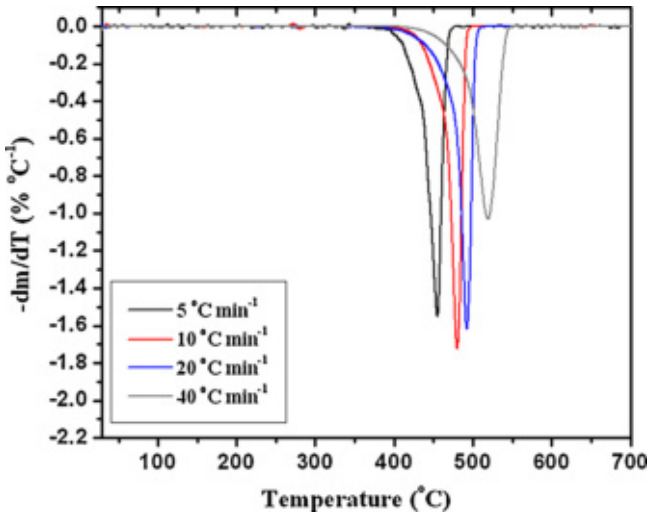

Fig. 2. DTG curves recorded at β = 5, 10, 20 and 40 °C min^{-1}, for non-isothermal decomposition process of a commercial silver nitrate in an argon (Ar) atmosphere.

approach, we need to be very careful, because if we rely only on the value of α_p in order to identify the reaction mechanism, our conclusions may lead us to a fundamental misreading of the reaction mechanism, because this approach is not sufficiently reliable for determining the proper kinetic model for the investigated process.

4.2. Isoconversional ('model-free') analysis

Fig. 3 shows the variation of the apparent activation energy (E_a), as a function of the extent of conversion (α), according to the Friedman (FR) (differential), Kissinger–Akahira–Sunose (KAS) (integral), Ozawa–Flynn–Wall (OFW) (integral) and Tang (T) (integral) isoconversional methods, respectively.

It can be observed from Fig. 3 that all isoconversional methods show a very similar variation of E_a as a function of α. In addition, the lower values of E_a were identified in the case of using the FR method, while the highest values of E_a were observed in the case of application OFW method. On the other hand, in a general sense, all values of E_a, which were calculated by the integral methods give

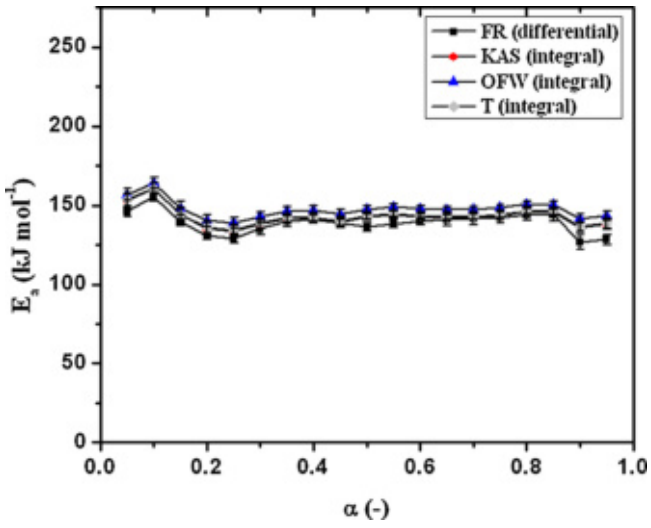

Fig. 3. The variation of the apparent activation energy (E_a), as a function of the extent of conversion (α), according to the Friedman (FR) (differential), Kissinger–Akahira–Sunose (KAS) (integral), Ozawa–Flynn–Wall (OFW) (integral) and Tang (T) (integral) isoconversional methods, for non-isothermal decomposition process of a commercial silver nitrate in an argon (Ar) atmosphere.

a very good mutual agreement (in the sense that there is no significant deviation of E_a values, calculated using different integral isoconversional methods, at each of the observed α value (Fig. 3)). It is possible that the use of a similar numerical evaluation of an integral equation (Eq. (3)) in the above isoconversional methods (KAS, OFW and T) give similar values of E_a.

Fig. 3 shows that the value of E_a increases from 153.1 up to 160.5 kJ mol^{-1} (with the values of E_a observed from KAS method) in the conversion range of $0.05 \leq \alpha \leq 0.10$. This behavior probably indicates on the reaction pathway which includes two independent parallel reaction systems. Namely, the first reaction path may includes the evaporation of the crystallization water and additional phase transformations of silver nitrate, while the second reaction path probably involves the formation of silver oxide (Ag_2O), during the thermal decomposition of $AgNO_3$ (Fig. 1). After $\alpha = 0.10$, we have a decrease in E_a values, with an increasing of α values, until the value of approximately $\alpha = 0.20$ (from 160.5 kJ mol^{-1} to 135.3 kJ mol^{-1}). Identified changes in the value of E_a in the range of 160.5–135.3 kJ mol^{-1} (Fig. 3) are in good agreement with the range of E_a changes (118–180 kJ mol^{-1}) during thermal decomposition of Ag_2O [64,65]. This reaction occurs in the temperature range where the rather broad endothermic peak stands in Fig. 1. Above the conversion value of $\alpha = 0.20$, we have a wide range of the extent of conversion values (up to $\alpha = 0.85$), where there is a significant stabilization in the value of E_a, so that here we can expect the further proceeding of silver oxide decomposition (maybe in the form of *dissociative* evaporation) [64] together with release of oxygen and nitrogen dioxide (NO_2), which values of the partial pressures may affect on the creation of final mechanistic scheme of the investigated process. In conversion range of approximately $0.15 \leq \alpha \leq 0.85$, the formation of silver particles can be expected on the side of higher temperatures and at higher values of α (Fig. 3). In the above mentioned conversion range ($\alpha = 0.15$–0.85), the E_a value can be taken as constant, so by the application of different isoconversional methods, the following average values of the apparent activation energy were obtained: $E_a^{FR} = 138.8 \pm 2.9$ kJ mol^{-1}, $E_a^{KAS} = 141.6 \pm 2.6$ kJ mol^{-1}, $E_a^{OFW} = 146.5 \pm 2.6$ kJ mol^{-1} and $E_a^{T} = 142.1 \pm 2.6$ kJ mol^{-1}, respectively (Fig. 3). It is interesting to note here that the above obtained values of E_a in the case of decomposition process of commercial silver nitrate under argon atmosphere, are very close to the value of E_a (137 kJ mol^{-1}), which is obtained in the case of the same process, but with one strike difference, where in the latter case, the nitrogen was used as carrier gas [18]. With nitrogen as carrier gas, it was found that the decomposition proceeds through the chemical rate controlled process, depending on the reaction temperature [18]. Therefore, it is important to determine a reliable mechanism of decomposition in an inert atmosphere of argon gas and then compare the resulting mechanism with a mechanism that exists in an inert nitrogen atmosphere, thereby drawing conclusions about the impact of the reaction atmosphere on the reaction mechanism of the tested compound.

According to the method proposed by Vyazovkin (Eqs. (8) and (9)) [32], the dependence of the *effective* activation energy, $E_{a,\alpha}$, on α can be evaluated, with eliminated systematic errors in E_a. Fig. 4 shows $E_{a,\alpha}$-dependency estimated by the application of Vyazovkin's advanced non-linear procedure, in the case of non-isothermal decomposition process of commercial silver nitrate, in an argon atmosphere.

It can be seen from Fig. 4 that the values of E_a exhibit exactly the same trend with increasing of α values, as in the case of other isoconversional methods presented in Fig. 3. The average value of E_a for $\alpha = 0.15$–0.85 calculated by the Vyazovkin's advanced 'model-free' approach was $E_a^V = 141.3$ kJ mol^{-1} (Fig. 4). This value is almost consistent with the value of E_a calculated by the KAS method (141.6 kJ mol^{-1}) (see above). Based on the obtained results, the

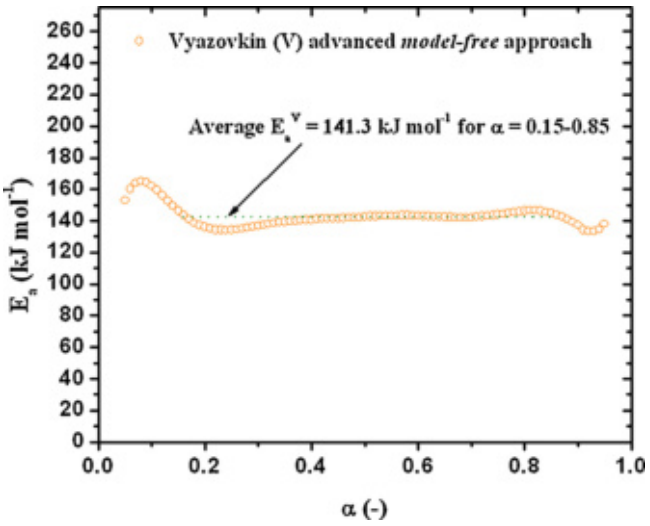

Fig. 4. The $E_{a,\alpha}$-dependency estimated by the application of Vyazovkin's advanced "model-free" procedure, in the case of non-isothermal decomposition process of commercial silver nitrate, in an argon atmosphere.

determination of reaction mechanism function can be performed in the conversion range where E_a value does not vary significantly with α. Because of this fact, the further kinetic analysis will be carried out in the conversion range of $0.15 \leq \alpha \leq 0.85$.

4.3. Analysis of the critical temperature (T_c) of non-isothermal decomposition process of commercial silver nitrate

Based on the results obtained from the isoconversional analysis, we can calculate the critical temperature (T_c), for investigated decomposition process, using the corresponding data of thermo-analytical measurements. Fig. 5 shows the functional relationship between the onset (initial) (T_i) temperatures and the values of heating rate (β) used in thermo-analytical measurements. In addition, the same figure (Fig. 5) also shows the mathematical expression

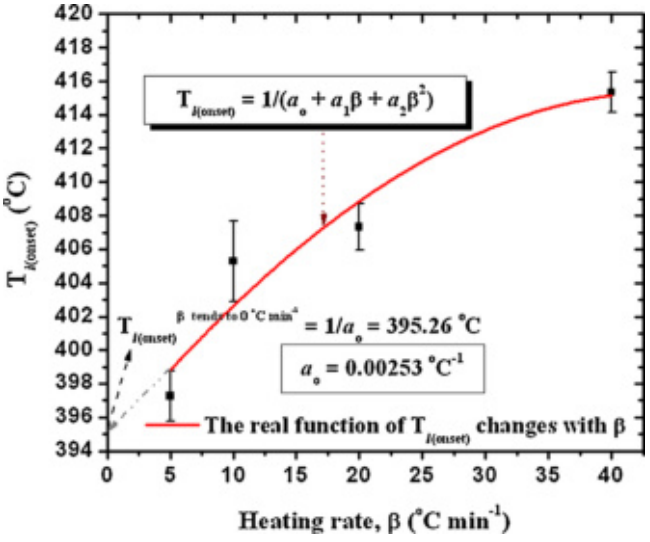

Fig. 5. The functional relationship between the onset (initial) ($T_{i(onset)}$) temperatures and the values of heating rate (β) used in thermo-analytical measurements; the same figure, also shows the mathematical expression that connects $T_{i(onset)}$ and β ($T_{i(onset)} = 1/(a_0 + a_1 \cdot \beta + a_2 \cdot \beta^2)$, where a_0, a_1 and a_2 represents the numerical coefficients), where the reciprocal value of the coefficient a_0 is equal to $T_{i(onset)}^{\beta \to 0}$ (the extrapolated onset temperature at $\beta \to 0\,^{\circ}\mathrm{C\,min^{-1}}$) ($T_{i(onset)}^{\beta \to 0} = 1/a_0$).

that connects T_i and β ($T_{i(onset)} = 1/(a_0 + a_1 \cdot \beta + a_2 \cdot \beta^2)$, where a_0, a_1 and a_2 represents the numerical coefficients), where the reciprocal value of the coefficient a_0 is equal to $T_i^{\beta \to 0}$ (the extrapolated onset temperature at $\beta \to 0\,^{\circ}C\,min^{-1}$) ($T_i^{\beta \to 0} = 1/a_o = 395.26\,^{\circ}C$; $a_0 = 0.00253\,^{\circ}C^{-1}$) ($T_i^{\beta \to 0}$ in Fig. 5 is marked with a gray dash dot–dot arrow). The data (the experimental T_i values (397.26 °C (5 °C min^{-1}), 405.28 °C (10 °C min^{-1}), 407.32 °C (20 °C min^{-1}) and 415.36 °C (40 °C min^{-1}) are indicated in Fig. 5 with dots in the form of black squares, including the experimentally obtained errors, expressed as the error bars) (Fig. 5)) are fitted to equation $T_{i(onset)} = 1/(a_0 + a_1 \cdot \beta + a_2 \cdot \beta^2)$ (the full continuous red line in Fig. 5) by the non-linear least-squares method, in the numerical calculations on a computer.

Using Eq. (14), with the known value of E_a obtained by applying the Ozawa–Flynn–Wall (OFW) isoconversional method ($E_a^{OFW} = 146.5$ kJ mol^{-1}), the critical temperature (T_c) for decomposition process of commercial silver nitrate can be calculated. The calculated value of the critical temperature (T_c) for the non-isothermal decomposition process of commercial silver nitrate in an argon atmosphere was $T_c = 422.74\,^{\circ}C$. If we look at Fig. 1 we should perceive that the avaluated value of T_c (422.74 °C) actually lies in the experimental temperature range in which we assume that the decomposition of silver oxide (Ag_2O) occurs, according to the equation:.

$$Ag_2O_{(s)} \rightarrow 2Ag_{(s)} + 1/2O_{2(g)}, \quad (34)$$

where Ag_2O is very unstable above 400 °C, so we can assume that the reaction under Eq. (34) in the overall reaction scheme:

$$2AgNO_{3(s)} \rightarrow Ag_2O_{(s)} + 2NO_{2(g)} + \tfrac{1}{2}\,O_{2(g)},$$
$$\downarrow$$
$$2NO_{(g)} + O_{2(g)} \quad (35)$$

may be the *main reaction stage* in the production of metal silver in argon-rich atmosphere, so it is of great importance to determine a reliable mechanism in the processing of silver particles, and then compare the results with the behavior of the same system in other reaction atmospheres such as inert atmosphere of nitrogen (N_2), and in purely reduction atmospheres in H_2, CO and C_2H_4 gases.

The resulting critical temperature $T_c = 422.74\,^{\circ}C$ is in fairly good agreement (in the sense of close values) with starting temperature of thermal decomposition process of the Ag_2O phase into Ag and oxygen (380–400 °C) [66], but lower than the starting temperature of Ag_2O decomposition in air atmosphere (300 °C) [67], for about 100 °C. An important physical consequence of the obtained value of T_c lies in the fact that the thermal stability in considered case refers not the stability of nitrate precursor crystal structure but on the precursor's *optimum space geometry*, because nitrate precursor can, before follow its decomposition, to assume several possible types of "*chemical species*" in transition state. Therefore, the rate of Ag_2O formation will largely depends on the occurrence of *one chemical species* whose spatial geometry is the best optimized, where the optimization affected by the length of chemical bonds in these species.

4.4. The model-fitting analysis

4.4.1. The capability test for initial estimation of the decomposition mechanism

A first screening of the kinetic mechanisms can be accomplished by using a Coats-Redfern (CR) kinetic method (Eq. (11)). Accordingly, at a specific heating rate, the E_a value can be estimated for various $g(\alpha)$ kinetic functions [19,20,23,35,37], by plotting of $\ln[g(\alpha)/T^2]$ versus $1/T$, according to Eq. (11). It was found that at all of the observed heating rates, there are several statistically equivalent kinetic models, which are grouped into the appropriate types of reaction models and they are as follows: (a) the power law kinetic models (nucleation models) (P2/3, P2, P3 and P4 (P*n*)), (b) the reaction-order kinetic model (zero-order, (R1/F0)) and (c) The diffusion kinetic models, D1, D2 and D4 (Ginstling–Brounshtein)

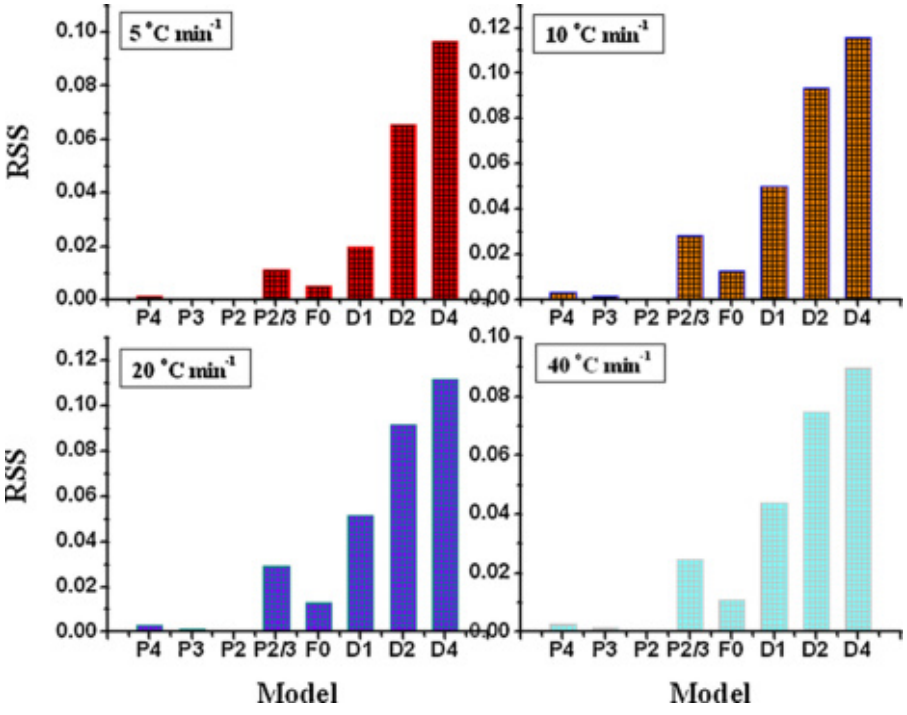

Fig. 6. The graphical representation in the form of statistical bars between the calculated values of the residual sum of squares (RSS) and the tested reaction models (P4, P3, P2, P2/3, F0, D1, D2 and D4), at the heating rates of 5, 10, 20 and 40 °C min^{-1}.

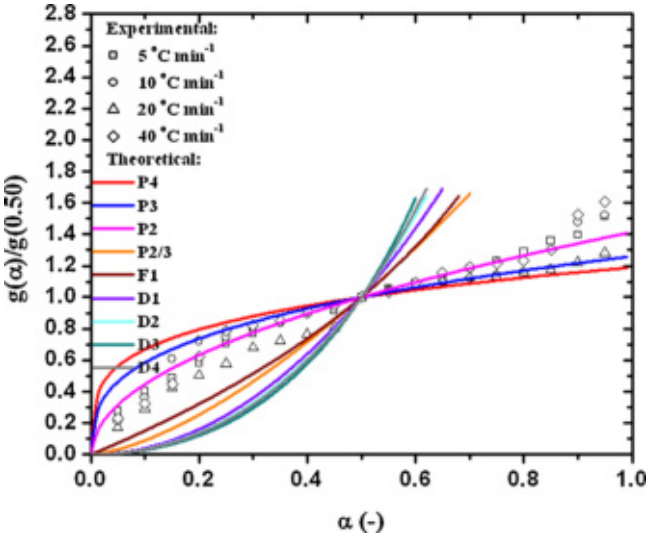

Fig. 7. Theoretical master plot curves in the integral form for the different kinetic models and the experimental data at the different heating rates (5, 10, 20 and 40 °C min^{-1}).

(Dn) (one-, two-, and three-dimensional diffusion, respectively). All models are characterized by the high values of Adj. R-square (R^2). Fig. 6 shows the graphical representation in the form of statistical bars between the calculated values of the residual sum of squares (RSS) and the tested reaction models (P4, P3, P2, P2/3, F0, D1, D2 and D4), at the heating rates of 5, 10, 20 and 40 °C min^{-1}.

It can be seen from Fig. 6 that the lowest values of the RSS have the models P4, P3, P2, where the most notable is the P2 model, with extremely low values of RSS, at all heating rates. For a given reaction model (model P2), the highest value of F-test [23] was obtained.

This initial finding was further investigated using the master plots method presented in Section 3.1.4.1. In accordance with Eqs. (16) and (17), the typical plots of $g(\alpha)/g(0.50)$ for investigated decomposition process appear in Fig. 7. For construction of $g(\alpha)/g(0.50)$ curves, the apparent activation energy calculated from Vyazovkin's method was used.

From the results presented in Fig. 7, we can see that at all heating rates, the experimental points are grouped on or around the theoretical curve for P2 kinetic model. Small deviations of the experimental points from the theoretical curve occur at very high values of conversion (for $\alpha \geq 0.90$). These results verified that the P2 kinetic model probably best describes the investigated decomposition process, so that the observed reaction model will be subject to further review.

In order to test the validity of the considered kinetic model, the composite integral and differential methods (I) were used in further kinetic analysis. The conversion range used in the calculation procedure was $0.15 \leq \alpha \leq 0.85$. In this kinetic analysis, the power law kinetic models, P4, P3, P2, and P2/3 were considered.

Table 2 shows the values of the pre-exponential factor (A) and the apparent activation energy (E_a), together with values of Adj. R-square (R^2) and the residual sum of squares (RSS), for considered kinetic models (P4, P3, P2, and P2/3), calculated by the composite integral and differential methods, respectively.

It can be seen from Table 2 that the kinetic model P2 gives the highest value of R^2 and the lowest value of RSS in both composite methods, where the calculated values of E_a in the case of both methods (139.7 and 141.5 kJ mol^{-1}, respectively), are in very good agreement with the values of E_a calculated by applying the Vyazovkin advanced isoconversional method ($E_a^V = 141.3$ kJ mol^{-1}) and other conventional isoconversional methods (see above).

Table 2
The results of the composite integral and differential methods (I) (Eqs. (12) and (13)) for tested power law kinetic models, P4, P3, P2, and P2/3, in the case of the non-isothermal decomposition process of commercial silver nitrate in an argon atmosphere.

Model	Composite integral method (I)			
	A (min^{-1})	E_a (kJ mol^{-1})	R^2 [b]	RSS [c]
P4	5.192×10^8	131.9	0.89222	1.46366
P3	7.366×10^8	134.5	0.92040	1.09095
P2 [a]	1.481×10^9	139.7	0.95635	0.62745
P3/2	9.547×10^{10}	171.0	0.76856	6.09231
	Composite differential method (I)			
	A (min^{-1})	E_a (kJ mol^{-1})	R^2 [b]	RSS [c]
P4	3.340×10^8	133.7	0.94966	0.66091
P3	6.197×10^8	136.3	0.96041	0.57361
P2 [a]	1.799×10^9	141.5	0.97061	0.31089
P3/2	2.842×10^{11}	172.7	0.69579	8.98393

[a] Statistical best selected model to describe the decomposition process.
[b] Adj. R-square.
[c] The residual sum of squares.

4.4.2. Estimation of the invariant kinetic parameters for investigated decomposition process

Furthermore, the IKP method was used for evaluation the "true" kinetic model, including the corresponding "real" values of the kinetic parameters (A and E_a). In the initial stage of analysis, the values of ln$A$ and E_a were calculated using the CR method at the different heating rates, for various $g(\alpha)$ kinetic functions [19,20,23,35,37]. Using Eq. (18), the existence of the compensation effect between ln$A$ and E_a was checked. Fig. 8 shows the real existence of the compensation effect for the non-isothermal decomposition process of commercial silver nitrate in an argon atmosphere.

The slopes and intercepts of these lines give the compensation parameters b_ν^* and a_ν^*, at each heating rate. Since the intersection of these lines is dependent on experimental conditions, the calculation of the invariant kinetic parameters is performed using the supercorrelation relation (Eq. (19)). The result appears in Fig. 9 and shows a very good straight line ($R^2 = 0.99215$) for the investigated process.

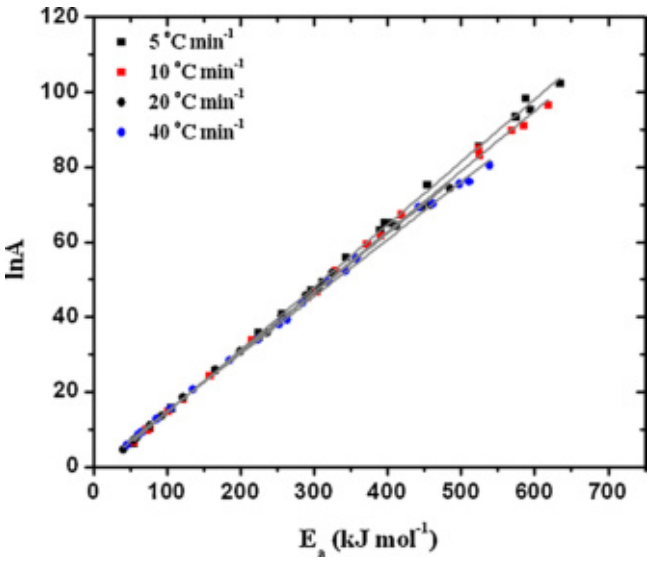

Fig. 8. Typical compensation relationships for non-isothermal decomposition process of a commercial silver nitrate in an argon (Ar) atmosphere.

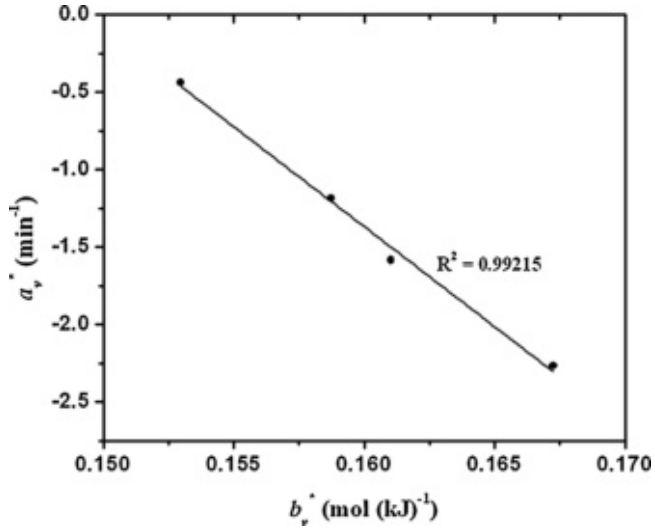

Fig. 9. The supercorrelation relation for non-isothermal decomposition process of a commercial silver nitrate in an argon (Ar) atmosphere.

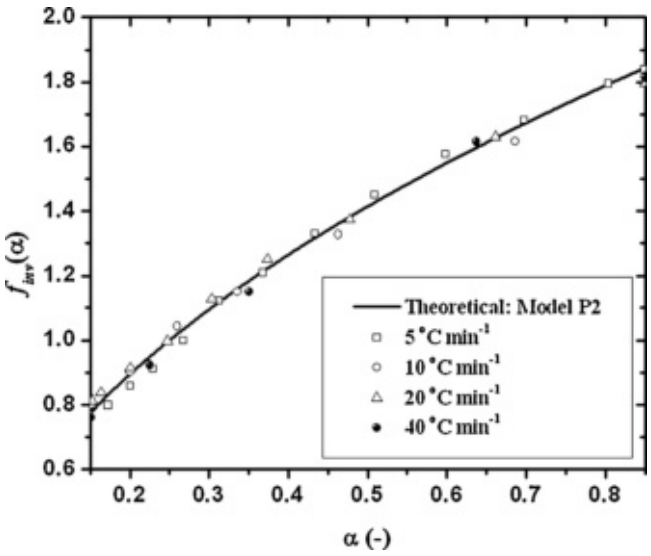

Fig. 10. The comparison between the estimated $f_{inv}(\alpha)$ function with calculated A_{inv} and $E_{a,inv}$ values (Eq. (20)) and theoretical $f(\alpha)$ function for P2 kinetic model ($f(\alpha) = 2\alpha^{1/2}$), in the conversion interval of $0.15 \leq \alpha \leq 0.85$.

In this way, the existence of a supercorrelation relation allows us to calculate A_{inv} and $E_{a,inv}$ from the intercept and the slope, respectively. The following values of the invariant kinetic parameters were obtained: $A_{inv} = 2.404 \times 10^8$ min^{-1} and $E_{a,inv} = 129.2 \pm 6.6$ kJ mol^{-1}. The obtained value of $E_{a,inv}$ is slightly lower than the values of E_a calculated by using different isoconversional methods. The observed value of $E_{a,inv}$ is the nearest to value of E_a calculated using the Friedman method (138.8 kJ mol^{-1}). On the other hand, the obtained value of A_{inv} (2.404×10^8 min^{-1}) is for one order of magnitude lower than corresponding values of A calculated by both composite methods, bearing in mind the kinetic model P2 ($\times 10^9$ (Table 2)). However, it should be mentioned here that was not observed huge fluctuations in the values of E_a obtained by different kinetic methods, taking into account the fact that the values of $E_{a,inv}$ can vary by more than 50% [23,68]. We must mention here the important fact that there is no significant difference between the values of the apparent activation energy calculated by IKP method and the Vyazovkin (V) advanced isoconversional method, which can be directly checked from the relation [69]:.

$$e[\%] = \frac{E_a(V-\text{advanced})_{iso} - E_a(IKP)}{E_a(V-\text{advanced})_{iso}} \cdot 100$$

$$= \frac{141.3 - 129.2}{141.3} \cdot 100 = 8.6\%, \quad (36)$$

which is quite satisfactory result because the observed difference is less than 10%.

4.5. Estimation of the most probable decomposition mechanism

According to previous findings, in order to estimate the reaction model that best describes the experimental data, the invariant kinetic function $f_{inv}(\alpha)$ was estimated from Eq. (20), using the previously calculated values of the invariant kinetic parameters, A_{inv} and $E_{a,inv}$. Fig. 10 shows the comparison between the estimated $f_{inv}(\alpha)$ function with calculated A_{inv} and $E_{a,inv}$ values (Eq. (20)) and theoretical $f(\alpha)$ function for P2 kinetic model ($f(\alpha) = 2\alpha^{1/2}$), in the conversion interval from $\alpha = 0.15$ to $\alpha = 0.85$.

From Fig. 10 we can clearly see the matching between $f_{inv}(\alpha)$ function at various heating rates (symbols), with a theoretical function $f(\alpha)$ corresponding to the P2 reaction model (the full black line).

To check the accuracy of the proposed model that describes the experimental data, we were used Eqs. (21) and (22) to perform the numerical reconstruction of the reaction model in the integral form, $g(\alpha)$, for the investigated decomposition process. The numerical calculations were performed in the conversion range, which corresponds to the conversion ranges used in isoconversional analysis ($0.05 \leq \alpha \leq 0.95$).

Fig. 11 shows the comparison between the numerically reconstructed $g(\alpha)$ functions, using Eqs. (21) and (22) at the different heating rates (5, 10, 20 and 40 °C min^{-1}) (*symbols*) and theoretical $g(\alpha)$ functions for the group of nucleation reaction models (the power law models: P4, P3, P2 and P2/3) (*colored solid lines*).

From Fig. 11 we can see that going over the value $\alpha = 0.15$ until the approximately $\alpha \approx 0.90$, there is a good agreement between the numerically reconstructed functions $g(\alpha)$ and the theoretical function of the reaction mechanism corresponding to the P2 kinetic model. This result confirms the previously established hypothesis that the kinetic model P2 is actually the best model to describe

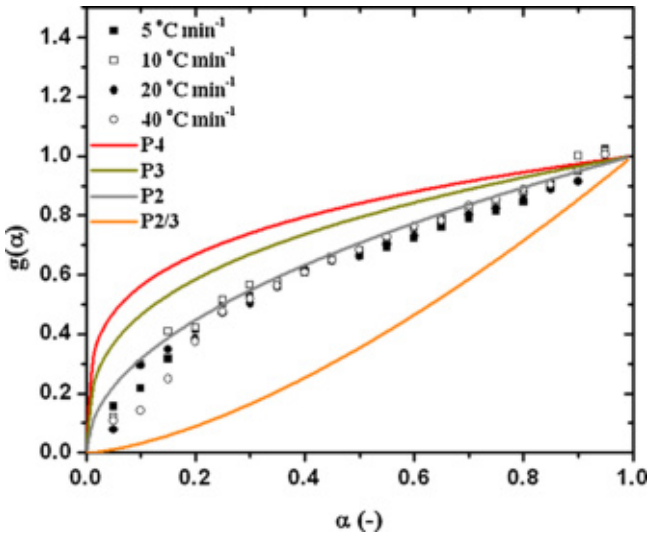

Fig. 11. The comparison between the numerically reconstructed $g(\alpha)$ functions, using Eqs. (21) and (22) at the different heating rates (5, 10, 20 and 40 °C min^{-1}) (symbols) and theoretical $g(\alpha)$ functions for the group of nucleation reaction models (the power law models: P4, P3, P2 and P2/3) (the colored solid lines).

Table 3
The values of the rate constants, $k_{critical}$ and $E_a \cdot (\beta)^p_{const.}/R \cdot T_p^2$, and the pre-exponential factor (A), calculated by using Eqs. (15), (23) and (24), for the non-isothermal decomposition process of commercial silver nitrate in an argon atmosphere.

β (°C min^{-1})	$k_{critical}$ (min^{-1}) [a]	$E_a \cdot (\beta)^p_{const.}/R \cdot T_p^2$ (min^{-1}) [a]	A (min^{-1}) [a]
5	0.05629	0.16460	1.948×10^9
10		0.30725	1.626×10^9
20		0.59590	2.217×10^9
40		1.10978	1.814×10^9

[a] The power law model P2 ($f(\alpha) = 2\alpha^{1/2}$; $g(\alpha) = \alpha^{1/2}$ {$f(\alpha) = n \cdot \alpha^{(n-1)/n}$, where n is the constant ($n = 2$)}).

the decomposition process of commercial silver nitrate in an argon atmosphere, through the single-step mechanism.

After determined reaction mechanism and the evaluated "true" value of the apparent activation energy, we can now join the corresponding specific values of the pre-exponential factors and the rate constants. Using Eqs. (15), (23) and (24), the corresponding values of the rate constants, $k_{critical}$ and $E_a \cdot (\beta)^p_{const.}/R \cdot T_p^2$ ($k_{critical}$ which corresponds to T_c and $E_a \cdot (\beta)^p_{const.}/R \cdot T_p^2$, which corresponds to each value of T_p on the individual values of the heating rate (β), taking the values of the kinetic parameters calculated using the Kissinger method; the following values of the kinetic parameters were obtained: $A^{\text{Kissinger}} = 4.060 \times 10^9$ min^{-1} and $E_a^{\text{Kissinger}} = 145.0 \pm 1.9$ kJ mol^{-1}) and the pre-exponential factors (A) can be calculated.

Table 3 lists the value of $k_{critical}$ and also the values of $E_a \cdot (\beta)^p_{const.}/R \cdot T_p^2$ and A at the different heating rates ($\beta = 5$, 10, 20, and 40 °C min^{-1}), calculated by using Eqs. (15), (23) and (24), respectively.

From the obtained results for the rate constants $k_{critical}$ and $E_a \cdot (\beta)^p_{const.}/R \cdot T_p^2$, we can clearly see that the decomposition process rapidly accelerates from the starting value of $k_{critical}$ over the values of $E_a \cdot (\beta)^p_{const.}/R \cdot T_p^2$, where the maximum rate is achieved at the highest heating rate (40 °C min^{-1}) (Table 3). On the other hand, the values of A (Table 3) calculated by Eq. (24) at all heating rates, are in very good agreement with the values of A calculated by the composite integral and differential methods (I), for the kinetic model P2 (Table 2). These results clearly indicate on the accelerating model which represents the type of the process whose rate continuously increases with increasing the conversion values, and reaches its maximum at the very end of the process. In our case, the resulting silver particles can act as an individual autocatalytic nucleation centers. Therefore, we must develop in a more details the corresponding mechanistic scheme of the entire decomposition process.

4.6. The mechanistic interpretation of decomposition process

Generally, thermal decomposition reactions, which involve the single solid substance undergoes transformation to solid and gaseous products are usually governed by the laws of topochemical reactions. The kinetics of such reactions are dependent on two competing processes, namely, (a) the rate of formation of the product phase, and (b) the rate of growth of product nuclei. The kinetic conversion curve for investigated decomposition process at 20 °C min^{-1} (Fig. 12) reflects the absence of induction period (which indicates a gradual increase in α and is normally represented by the lower section of the curve) followed by a rapid increase in α (predominantly the middle section in Fig. 12, which is restricted by horizontal dashed lines) and in the rate of decomposition of silver oxide as the *active intermediate* compound to produce the metallic silver particles in the form of required final product.

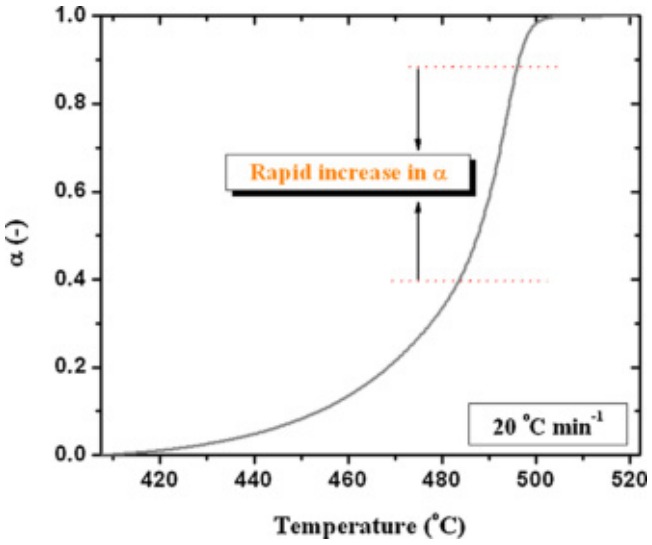

Fig. 12. The kinetic conversion (α–T) curve at $\beta = 20$ °C min^{-1}, for non-isothermal decomposition process of a commercial silver nitrate in an argon (Ar) atmosphere; the same figure shows the middle region of the conversion curve with a rapid increase in α values.

This (middle) section of the curve reflects the growth of the interfacial surface and the autocatalytic acceleration of the process concentrated on it. The upper section of the curve (Fig. 12) represents the retarding process due to the deepening of the reaction zone within the reacting substance and the reduction in its span. The reaction profile presented on considered α–T curve belongs to the accelerating models such as found the power law model P2 with topochemical constant $n = 2$. From the kinetic point of view, the dynamic (non-isothermal) approach, gives a better indication of the sample at any instant of time with respect to both temperature and the extent of conversion.

Based on the obtained values of kinetic parameters ($A_{inv} = 2.404 \times 10^8$ min^{-1}, $E_{a,inv} = 129.2$ kJ mol^{-1}) and evaluated topochemical constant, which is equal to 2, we can conclude that the non-isothermal decomposition process of commercial silver nitrate is essentially a surface-controlled process. In addition, based on the obtained value of the constant n, which is $n = 2$, we can derive unambiguous conclusion that the considered *power* indicates pure nucleus growth, where the new nuclei are formed thermally. On the other hand, considering that we have a lack of induction period, we can assume that the many small nuclei are formed, none of which grow to visible size. In considered case, the whole surface then nucleates rapidly and the kinetics of the remainder of the reaction depends on the rate at which the interface progresses. Therefore, we can assume that the small grain size and high temperature accelerate the grain growth. It should be noted that on the acceleration of silver particles growth process, can greatly affect the appearance of dislocations (or the stacking faults – these are mistakes occurring in the stacking sequence of close packed structures in solids (the plane separating two incorrectly juxtaposed layers is called stacking fault)) in crystal structure of silver oxide as the main intermediate compound. On the other hand, the value of n ($n = 2$) may indicates the "*magnitude of grain growth speeds*" and also growth dimensions. Taking into account the results of the rate constants at different heating rates (presented in Table 3) and established value of n, we may conclude that the growth rate increases with an increasing β (i.e. temperatures). In the growth stage, the grain growth is mainly dominated by the *grain boundary migration* [70]. Namely, it is possible that the appearance the stacking faults (dislocations) lowers *the activation energy* for the atoms on grain boundary, thereby

transforming them into grains, so the dislocations (or stacking faults) may act as the intermediary for the atom transforming from grain boundary to grains. Discussion presented above can be taken as an assumption on the possible direction of development of the investigated process, as the confirmation of the above assumptions, it is necessary to perform additional measurements (such as X-ray diffraction analysis, SEM analysis, etc.).

The physical justification for established model can be viewed in several items:

(i) The *activation energy* for the nucleus formation is the little lower than for the growth. This assumption has a reasonable basis in Fig. 4. In fact, if we look closely at Fig. 4, we can see the existence of "*valleys*" in the E_a values, in the range of low α values ($0.18 \leq \alpha \leq 0.32$). Thus, the contribution of each value of the *activation energy* for the formation of a single nucleus is reflected in the appearance of the *lower* values of the *effective* (*apparent*) activation energy in $E_{a,\alpha} - \alpha$ dependence in the investigated decomposition process. In this case, the overall rate can be represented by the modified Arrhenius-type equation in the form as:

$$k_{overall} = \exp\left(-\frac{\varepsilon_n}{RT}\right) \cdot \exp\left(-\frac{E_g}{RT}\right) \quad (37)$$

where $\exp(-\varepsilon_n/RT) = k_f$ and $\exp(-E_g/RT) = k_{gr}$ represent the rate of formation of nuclei and the rate of growth of nuclei, respectively.

(ii) The complexity of Eq. (37) (includes two exponential terms) may indicates that the nucleation and growth are occurring simultaneously at the beginning of the reaction, but at the higher values of α (and in the higher temperature regions), the growth process is enhanced relatively more than the nucleation (since it has the *higher activation energy*, which is generally reflected in *higher* values of E_a in Fig. 4, for $\alpha > 0.32$). This is reflected in constant $n = 2$, for power law kinetic model.

Generally, it is complicated to analyze E_a numerically, because both ε_n and E_g are usually unknown. On the basis of this review, we can only quantitative assume the value of ε_n, which should be a little lower than E_g, due to the fact that because ionic transport phenomena in polar silver salt, usually involves the transport of interstitial silver ions only, than the basic process of nuclei formation can be assumed to be a "migration" of silver ions to potential sites of nucleation (being the crystal defects).

It can be pointed out, that the morphology, sizes and size distribution of silver nanoparticles depends on several reaction conditions such as: the initial particle shapes (and concentration) of nitrate precursors, the experimental range of temperatures, type of carrier gas used, the heating rate used, etc. [71–73]. The power law kinetic model is natural, because in reality the nanoparticles are inevitably not fully identical due to the size and shape distribution, and for possible formation of a thin metal oxide layer. These factors result in a distribution of the kinetic parameters for nucleation and the kinetic model should be the *non-exponential*. In addition, both the the average size and size distribution of the crystallites in the sample are dependent on the growth temperature, consistent with surface-free energy considerations. The temperature necessary to maintain steady growth increases with the expansion of the crystallite's size. As the size distribution sharpens, the reaction temperature must be raised to maintain steady growth.

Conversely, if the size distribution begins to spread, the temperature required for slow steady growth drops. On the other hand, the presence of evolved gases during decomposition process may affects on the formation of interlayers. Therefore, we can assume that the presence of oxygen can causes the formation of Ag_2O interlayer. This can be checked by the EDX (Energy-dispersive X-ray) analysis, which is one of the goals of our future work, which is in preparation. If this reasoning be correct, the above measurements would probably reveal that the kinetics of oxide is close to a parabolic growth [74]. On the other hand, the development of other gases such as NO_2 (and probably *gas mixtures* ($NO + O_2$)) can cause the changes on sample surface in the beginning of the decomposition process. Some of the formed gas mixtures can be inert at the beginning of the process, while others may be very active in changing the sample surface. Therefore, at this time, the type of inert (carrier) gas can play a key role in the final morphology of the obtained silver particles.

Furthermore, the authors believe that the main differences between the nitrogen and argon as the inert gases lie in the degree of creation of specific types of defects, which may affect on the kinetics of the entire process, and thus the formation of the final product. Unlike oxygen and nitrogen (which can form the oxide and nitride), the argon probably can forms, in significantly amount, a specific defects (perhaps interstitial atoms) and on this way may affects on the global crystallization kinetics. The mentioned defects may cause some special behavior like density decrease and also influenced on the global crystallization kinetics at elevated temperatures. The influence of inert gases on the global crystallization kinetics and also their "degree of efficiency" probably can be determined from the relation that connects the "residence time" and corresponding diffusion parameters such as $t \propto X^2/D$, where X represents the diffusion distance and D represents the diffusion coefficient related to the mobility of the atoms. From this, it follows that the removal process should be a physical process. In that sense, the effect of D on the removal time seems to be important in the practical cases, when using the ultrasonic spray pyrolysis (USP) procedure.

In our previous paper [12,18], the use of nitrogen as a carrier gas during the non-isothermal decomposition of nitrate precursors, the silver nanoparticles of spherical (3D) shape were obtained, with a decomposition mechanism different from the mechanism established in this study. On the other hand, in the presence of the reducing agent such as hydrogen, there is a direct reduction in metallic silver (with a mixture of cylindrical, prismatic and spherical shapes of particles) [12,18,75] without creating the intermediate compounds. The confirmation of the established kinetic model for the current decomposition process was given in the [Supplementary Data] through the graphical interpretations in the various conversion areas, as the dependence of the kinetic models on the reaction time (x-axis is given on the timeline).

4.7. Kinetic prediction analysis

Assuming the single-step process, the predictions of the isothermal kinetics were performed at four different operating temperatures (T_o = 410.29, 445.27, 475.27, and 494.86 °C) with kinetic 'triplet' determined from the IKP method, and direct use of Eq. (25). Fig. 13 shows the isothermal predictions of decomposition process of commercial silver nitrate at different operating temperatures (410.29, 445.27, 475.27, and 494.86 °C) by application of Eq. (25).

We can see from Fig. 13 that for all the observed operating temperatures, the shape of α–t curves is identical, where the resulting shape of the curves corresponds to the shape of conversion curves attached to the accelerating reaction models, such as the power law models. This result confirms the fact that, if the process takes place through a single reaction stage in a rather wide range of α, we can expect that the isothermal and non-isothermal approaches to the decomposition process under study, will lead to the same end result, i.e., the same type of reaction mechanism. Also, we can see that the increase in the values of T_o leads to a drastic shortening of the *time duration* of the investigated process. So that the

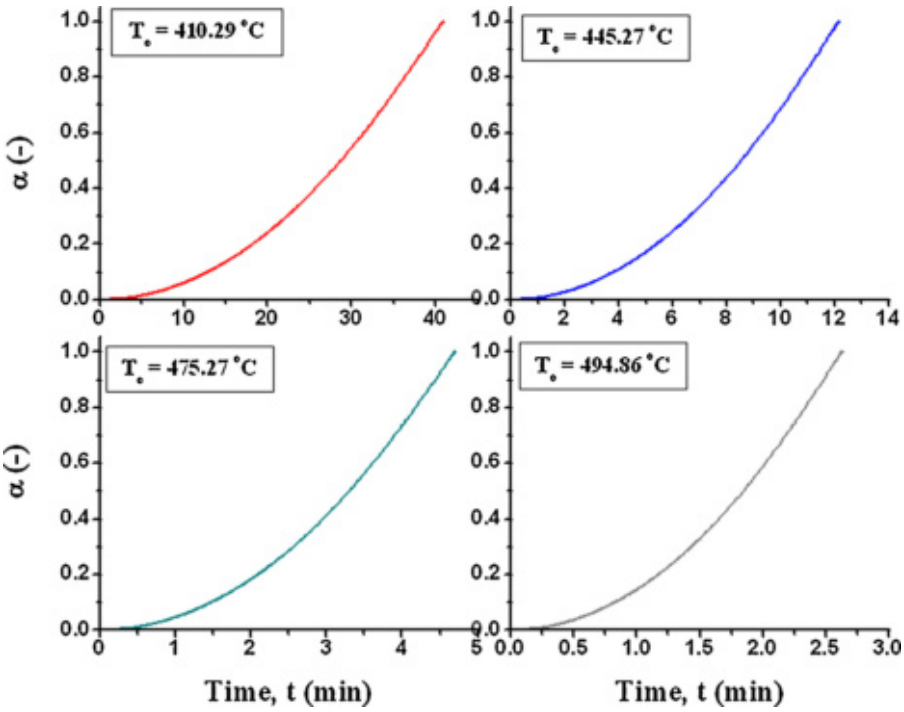

Fig. 13. The isothermal kinetic predictions of decomposition process of commercial silver nitrate at different operating temperatures (T = 410.29, 445.27, 475.27, and 494.86 °C) by application of Eq. (25).

temperature rise, undoubtedly rapidly accelerates the decomposition process (reactions are very temperature-sensitive).

In addition, Fig. 14 shows the "model-free predictions" of the investigated decomposition process, carried out at the heating rate of β = 10 °C min^{-1} at the considered operating temperatures (410.29, 445.27, 475.27, and 494.86 °C).

Also, we can see from Fig. 14, that α–t curves remain almost identical form at all the observed operating temperatures (410.29, 445.27, 475.27, and 494.86 °C). Also, in Fig. 14, we can also see that in the conversion range where we get a constant value of E_a ($0.15 \leq \alpha \leq 0.85$), all α–t curves have an area with a rapid increase in α values, which is typical for the power law model.

Overall, if we compare the results presented in Figs. 13 and 14, we can see that the shapes of α–t curves differ at all observed operating temperatures, while bearing in mind that the observed curves in Figs. 13 and 14 are evaluated by two different equations used for predictions. Namely the appearance of differences in shapes of α–t curves in Figs. 13 and 14 may arise from the fact that in the first case (Fig. 13), the presented approach does not allow the isolation of possibly attending elementary reactions in a complex reaction system. This approach rather gives a global kinetic picture of the investigated process through the single-step transformation, without considering the presence of the reaction sub-steps, if they really exist. On the other hand, in the second case (Fig. 14), the presented approach allows us to detect complex reaction system involving several steps with different E_a values, so that we should consider the investigated decomposition process through the effective kinetic parameters values, unless the mechanistic conclusions can be justified by the ancillary data.

In addition, the effective activation energy is generally a function of the temperature. Furthermore, even if the temperature is kept constant (the isothermal experiment), the relative contributions of the elementary steps (Fig. 4) to the overall rate of the process (Eq. (37)) can vary with α, undoubtedly resulting in the dependence of E_a on α (namely, this behavior can be clearly seen in Fig. 4).

Taking into account all the above facts, the isothermal thermoanalytical measurements together with surface characterization of the tested material will be carried out, and the results will be presented in our next paper.

Table 4 shows the values of lifetimes ($t_{5\%}$ and $t_{50\%}$) at the different operating temperatures (T_o = 410.29, 445.27, 475.27, and 494.86 °C), for the thermal decomposition process of commercial silver nitrate in an argon atmosphere. The corresponding values of the apparent activation energy ($E^{pred}_{a,5\%}$ and $E^{pred}_{a,50\%}$) were calculated from the relation $-\ln(t_{\alpha(\%)}) = const. - E^{pred}_{a,\alpha(\%)}/RT_o$ [20].

From Table 4 we may see that a temperature rise for about 85 °C, causing sudden shortening of *lifetime*, so at the highest value of T_o (494.86 °C), we can observe very low values of $t_{\alpha(\%)}$ (for T_o = 494.86 °C, the value of $t_{5\%}$ goes below 1 min). On the other hand, the calculated values of $E^{pred}_{a,5\%}$ and $E^{pred}_{a,50\%}$ (149.5 and 141.3 kJ mol^{-1}, respectively) are in very good agreement with the values of the apparent activation energy evaluated from the non-isothermal data (141.3 kJ mol^{-1}), where the appropriate matching of the given values occurs at $t_{50\%}$ (Table 4).

Table 4
The values of lifetimes ($t_{5\%}$ and $t_{50\%}$) for the different operating temperatures (T_o = 410.29, 445.27, 475.27, and 494.86 °C), in the case of thermal decomposition process of commercial silver nitrate in an argon atmosphere; the same table contains the calculated values of the apparent activation energy ($E^{pred}_{a,5\%}$ and $E^{pred}_{a,50\%}$), from the isothermal relation in the form: $-\ln(t_{\alpha(\%)}) = const. - E^{pred}_{a,\alpha(\%)}/RT_o$.

Lifetime, $t_{\alpha(\%)}$ (min)	T_o (°C)			
	410.29	445.27	475.27	494.86
$t_{5\%}$	9.00	2.20	0.85	0.50
$t_{50\%}$	29.00	8.50	3.25	1.85
$E^{pred}_{a,5\%}$ (kJ mol^{-1})			149.5	
$E^{pred}_{a,50\%}$ (kJ mol^{-1})			141.3	

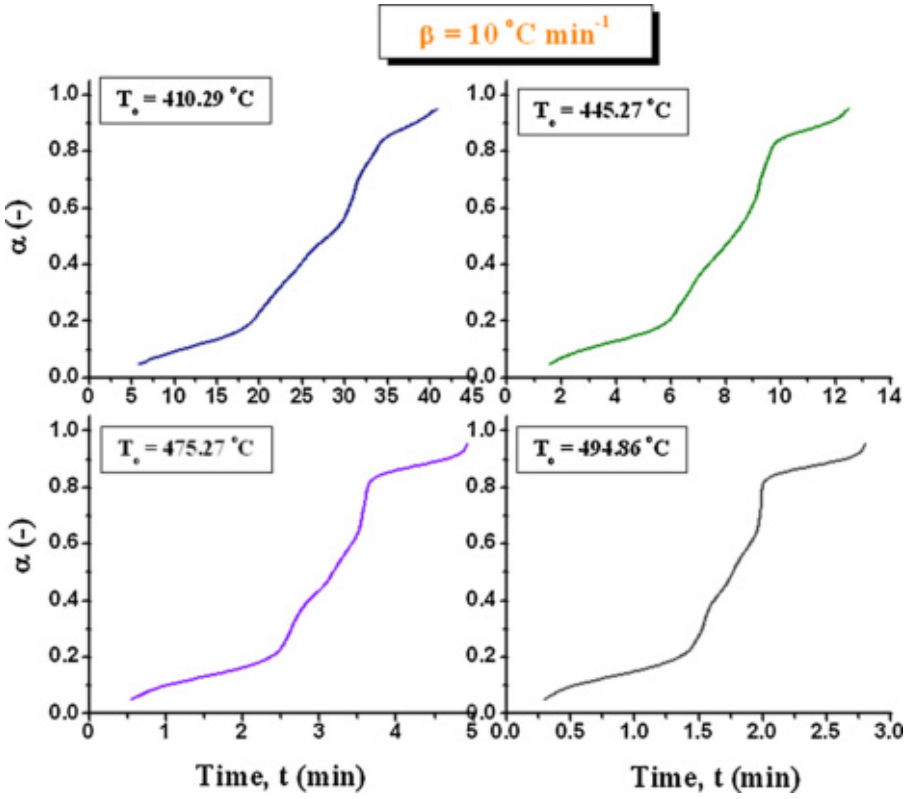

Fig. 14. The "model-free predictions" of the investigated decomposition process, performed at the heating rate of $\beta = 10\,^{\circ}C\,min^{-1}$, at the considered operating temperatures (T = 410.29, 445.27, 475.27, and 494.86 °C).

Therefore, only the power law kinetic model P2 (with $f(\alpha) = 2\alpha^{1/2}$) gives the value of E_a which is consistent with the value obtained from the isothermal conditions.

4.8. Thermodynamic considerations

After the determination of reaction model, we calculated other thermodynamic parameters using the selected thermodynamic equations (Eqs. (28)–(30)). Table 5 presents these results. The values of $\Delta H^{\neq\circ}$, $\Delta S^{\neq\circ}$ and $\Delta G^{\neq\circ}$ represent the overall values of thermodynamic parameters for the investigated decomposition process.

The entropy of activation ($\Delta S^{\neq\circ}$) value at all heating rates for decomposition process is negative. A negative value of $\Delta S^{\neq\circ}$ indicates a highly ordered activated complex and the degrees of freedom of rotation as well as of vibration is less than they in the non-activated complex. These results may indicate a "slow" stage [50]. Hence, the silver–oxygen bond secession can be interpreted as a slow stage of the process (where for the decomposition of silver oxide endothermic effects can occur, $\Delta H^{\neq\circ} > 0$). The positive values of $\Delta H^{\neq\circ}$ and $\Delta G^{\neq\circ}$ for the decomposition stage shows that it is connected with the introduction of heat and it is non-spontaneous process. The presented thermodynamic functions are in consistent with kinetic parameters.

Table 6 lists the values of the thermodynamic equilibrium constant (K_o) and the corresponding logarithmic values of K_o ($\log(K_o)$) at the different selected operating temperatures (126.85 °C (400 K), 226.85 °C (500 K), 326.85 °C (600 K) and 426.85 °C (700 K)), where these values are selected in such a way to include the "*lower*" temperature range (below the temperatures T_p (Table 1)) of the investigated decomposition process [76]. Also, Table 6 provides the values of thermodynamic parameters ($\Delta H^{\neq\circ}$, $\Delta S^{\neq\circ}$ and $\Delta G^{\neq\circ}$) calculated using Eqs. (31) and (32).

From Table 6 we can see that if we increase the temperature, then we are closer and closer to the value $K_o = 1$ ($\Delta G^{\neq\circ} = 0$, thermodynamic equilibrium; the value of $\Delta G^{\neq\circ}$ decreases with increasing of T (Table 6)). For selected temperatures, below T_p (Table 6), we can see that the value of $\Delta H^{\neq\circ}$ is still positive but much lower than the values of $\Delta H^{\neq\circ}$ which are shown in Table 5. In this way, we would be in the stage of "*initial degradation*" of precursors. On the other hand, in the current case, $\Delta S^{\neq\circ}$ changes the sign and becomes positive, which indicates a malleable activated complex that leads to a large number of degrees of freedom, leading to a "fast" stage. It should be noted that below 226 °C (~500 K; Table 6),

Table 5
Thermodynamic parameters ($\Delta H^{\neq\circ}$, $\Delta S^{\neq\circ}$ and $\Delta G^{\neq\circ}$) for the decomposition process of commercial silver nitrate in an argon atmosphere, at the different heating rates (β = 5, 10, 20 and 40 °C min^{-1}).

β (°C min^{-1})	$\Delta H^{\neq\circ}$ (kJ mol^{-1})	$\Delta S^{\neq\circ}$ (kJ mol^{-1} K^{-1})	$\Delta G^{\neq\circ}$ (kJ mol^{-1})
5	138.9	−0.12	224.0
10	138.7	−0.12	228.1
20	138.6	−0.12	227.5
40	138.4	−0.12	232.1

Table 6
The values of K_o, $\log(K_o)$, as well as the values of thermodynamic parameters ($\Delta H^{\neq\circ}$, $\Delta S^{\neq\circ}$ and $\Delta G^{\neq\circ}$) calculated using Eqs. (31) and (32), at the different selected operating temperatures (126.85 °C (400 K), 226.85 °C (500 K), 326.85 °C (600 K), and 426.85 °C (700 K)) for the investigated decomposition process.

T (K)	K_o	$\log(K_o)$	$\Delta H^{\neq\circ}$ (kJ mol^{-1})	$\Delta S^{\neq\circ}$ (kJ mol^{-1} K^{-1})	$\Delta G^{\neq\circ}$ (kJ mol^{-1})
400	1.98×10^{-16}	−36.158	33.3	0.40	120.3
500	1.47×10^{-8}	−18.035			75.0
600	8.06×10^{-4}	−7.123			35.5
700	4.77×10^{-1}	−0.740			4.3

the partial pressure of oxygen ($p(O_2)$) is probably fixed by the reaction, which is presented by Eq. (34) [76]. Therefore, the knowledge of the value of the partial pressure of oxygen in the reaction mixture is essential to the establishment of the thermodynamic equilibrium of the system [77]. Monitoring the above parameters during tests of thermal stability of nitrate precursors, together with a reliable description of the kinetic behavior under the influence of high temperatures, is of great importance for the industrial applications. This is necessary in order to better optimize the entire process of obtaining silver nanoparticles by the ultrasonic spray pyrolysis, where it has the advantage of being highly scalable and continuous [78].

5. Conclusions

The non-isothermal decomposition process of commercial silver nitrate used as the precursor for the USP procedure, was investigated by simultaneous TGA–DTA measurements at different heating rates (5, 10, 20 and 40 °C min^{-1}), in an argon atmosphere. We performed a detailed kinetic and thermodynamic analysis of the considered process, with special emphasis on the formation of a complete mechanistic scheme of the process, in an inert atmosphere of argon. It was found that the process under study can be described by the acceleratory power law kinetic model (P2), in the range of the extent of conversion values ($0.15 \leq \alpha \leq 0.85$), where the value of the apparent activation energy (E_a) can be considered as the constant (141.3 kJ mol^{-1}). A full kinetic 'triplet' and the complete mechanistic scheme of the investigated process were developed.

The temperature/conversion effects can affect on the rate and the apparent activation energy in the early stage of the current process, so that in this region the value of the apparent activation energy is reduced, which leads to an increase in the rate of process.

It is assumed that the main differences between the nitrogen and argon as the inert gases lie in the degree of creation of specific types of defects, which may affect on the kinetics of the entire process, and thus the formation of the final product. Unlike oxygen and nitrogen (which can form the oxide and nitride), the argon (Ar) probably can forms, in *significantly* amount, a specific defects (perhaps a interstitial atoms) and on this way may affects on the global crystallization kinetics. It is assumed that the process of removing the gases is a physical process.

The kinetic prediction analysis was shown that only the power law kinetic model P2 (with differential kinetic model function $f(\alpha) = 2\alpha^{1/2}$) gives the value of E_a which is consistent with the value obtained from the isothermal conditions. The emergence of various shapes of α–t curves at different operating temperatures (410.29, 445.27, 475.27, and 494.86 °C) obtained by the isothermal predictions using Eqs. (25) and (26) was discussed.

On the basis of correctly established value of the apparent activation energy, the pre-exponential factor and the changes of entropy, enthalpy and Gibbs free energy, the certain conclusions can be made concerning the mechanism and characteristics of the process, which play an important role in theoretical study and in an industrial application, concerning to formation of nanoparticles from an aerosol produced in an ultrasonic field.

Acknowledgements

The authors would also like to thank the Ministry of Science and Environmental Protection of Serbia, under the Project 172015 (Prof. Dr Bojan Janković) and DAAD Project No. 54392239 entitled: "Numerical simulation of Ag-nanoparticle formation from aerosol" (Prof. Dr Bojan Janković, Dr.-Ing. Srećko Stopić, M.Sc.-Ing. Jelena Bogović, and Dr.-Ing. Bernd Friedrich).

Appendix A. Supplementary data

Supplementary data associated with this article can be found, in the online version, at http://dx.doi.org/10.1016/j.cep.2014.06.002.

References

[1] V.L. Colvin, M.C. Schlamp, A. Alivisatos, Light emitting diodes made from cadmium selenide nanocrystals and a semiconducting polymer, Nature 370 (1994) 354–357.
[2] Y. Wang, N. Herron, Nanometer-sized semiconductor clusters: materials synthesis, quantum size effects, and photophysical properties, J. Phys. Chem. 95 (1991) 525–532.
[3] G. Schmid, Large clusters and colloids. Metals in the embryonic state, Chem. Rev. 92 (1992) 1709–1727.
[4] A.J. Hoffman, G. Mills, H. Yee, M. Hoffmann, Q-sized cadmium sulfide: synthesis, characterization, and efficiency of photoinitiation of polymerization of several vinylic monomers, J. Phys. Chem. 96 (1992) 5546–5552.
[5] J.F. Hamilton, R. Baetzold, Catalysis by small metal clusters, Science 205 (1979) 1213–1220.
[6] H.S. Mansur, F. Grieser, M.S. Marychurch, S. Biggs, R.S. Urquhart, D. Furlong, Photoelectrochemical properties of 'q-state' cds particles in arachidic acid Langmuir–Blodgett films, J. Chem. Soc. Faraday Trans. 91 (1995) 665–672.
[7] S. Mayavan, J.-B. Sim, S.-M. Choi, Easy synthesis of nitrogen-doped graphene-silver nanoparticle hybrids by thermal treatment of graphite oxide with glycine and silver nitrate, Carbon 50 (2012) 5148–5155.
[8] S.L. Nair, T.C. Laurencin, Silver nanoparticles: synthesis and therapeutic applications, J. Biomed. Nanotechnol. 3 (2007) 301–316.
[9] T.C. Pluym, Q.H. Powell, A.S. Gurav, T.L. Ward, T.T. Kodas, L.M. Wang, H.D. Glicksman, Solid silver particle production by spray pyrolysis, J. Aerosol Sci. 24 (1993) 383–392.
[10] E. Ide, S. Angata, A. Hirose, K. Kobayashi, Metal–metal bonding process using Ag metallo-organic nanoparticles, Acta Mater. 53 (2005) 2385–2393.
[11] D. Majumdar, H. Glicksmann, T. Kodas, Generation and sintering characteristics of silver–copper (II) oxide composite powders by spray pyrolysis, Powder Technol. 110 (2000) 76–81.
[12] S. Stopić, B. Friedrich, T. Volkov-Husovic, K. Raić, Mechanism and kinetics of nanosilver formation by ultrasonic spray pyrolysis – progress report after successful up-scaling (Part 2), Metall 65 (2011) 93–96.
[13] S. Stopić, S. Gürmen, B. Friedrich, Mechanism of synthesis of nanosized spherical cobalt powder by ultrasonic spray pyrolysis, J. Metall. 11 (2005) 65–73.
[14] Z. Marinković, L. Mančić, R. Marić, O. Milošević, Preparation of nanostructured Zn–Cr–O spinel powder by ultrasonic spray pyrolysis, J. Eur. Ceram. Soc. 21 (2001) 2051–2055.
[15] B. Xia, W. Lengorro, K. Okyama, Preparation of nickel powders by of nickel formate, J. Am. Ceram. Soc. 84 (2001) 1425–1432.
[16] G. Messing, S. Zhang, G. Jayanthi, Ceramic powder synthesis by spray pyrolysis, J. Am. Ceram. Soc. 76 (1993) 2707–2726.
[17] S. Stopić, B. Friedrich, P. Dvorak, Synthesis of nanosized spherical silver powder by ultrasonic spray pyrolysis, Metall 60 (2006) 377–382.
[18] S. Stopić, B. Friedrich, T. Volkov-Husovic, K. Raić, Mechanism and kinetics of nanosilver formation by ultrasonic spray pyrolysis – progress report after successful up-scaling, Metall 64 (2010) 419–426.
[19] A. Khawam, D.R. Flanagan, Solid state kinetic models: basics and mathematical fundamentals, J. Phys. Chem. B 110 (2006) 17315–17328.
[20] S. Vyazovkin, C.A. Wight, Model-free, model-fitting approaches to kinetic analysis of isothermal and nonisothermal data, Thermochim. Acta 340–341 (1999) 53–68.
[21] A.K. Burnham, L.N. Dinh, A comparison of isoconversional and model-fitting approaches to kinetic parameter estimation and application predictions, J. Therm. Anal. Calorim. 89 (2007) 479–490.
[22] S. Vyazovkin, C.A. Wight, Isothermal and nonisothermal kinetics of thermally stimulated reactions of solids, Int. Rev. Phys. Chem. 17 (3) (1998) 407–433.
[23] S. Vyazovkin, A.K. Burnham, J.M. Criado, L.A. Pérez-Maqueda, C. Popescu, N. Sbirrazzuoli, ICTAC Kinetics Committee recommendations for performing kinetic computations on thermal analysis data, Thermochim. Acta 520 (2011) 1–19.
[24] C.D. Doyle, Kinetic analysis of thermogravimetric data, J. Appl. Polym. Sci. 5 (1961) 285–292.
[25] T. Ozawa, A new method of analyzing thermogravimetric data, Bull. Chem. Soc. Jpn. 38 (1965) 1881–1886.
[26] J.H. Flynn, L.A. Wall, General treatment of the thermogravimetry of polymers, J. Res. Natl. Bur. Stand. 70A (1966) 487–523.
[27] S. Vyazovkin, N. Sbirrazzuoli, Isoconversional kinetic analysis of thermally stimulated processes in polymers, Macromol. Rapid Commun. 27 (2006) 1515–1532.
[28] H.E. Kissinger, Reaction kinetics in differential thermal analysis, Anal. Chem. 29 (1957) 1702–1706.
[29] T. Akahira, T. Sunose, Method of determining activation deterioration constant of electrical insulating materials, Res. Rep. Chiba Inst. Technol. (Sci. Technol.) 16 (1971) 22–31.
[30] W. Tang, Y. Liu, H. Zhang, C. Wang, New approximate formula for Arrhenius temperature integral, Thermochim. Acta 408 (2003) 39–43.

[31] H.L. Friedman, Kinetics of thermal degradation of char-forming plastics from thermogravimetry: application to a phenolic plastic, J. Polym. Sci. C 6 (1963) 183–195.
[32] S. Vyazovkin, Modification of the integral isoconversional method to account for variation in the activation energy, J. Comp. Chem. 22 (2001) 178–183.
[33] A.W. Coats, J.P. Redfern, Kinetic parameters from thermogravimetric data, Nature 201 (1964) 68–69.
[34] M. Tunc, H. Ersahan, S. Yapici, S. Colak, Dehydration kinetics of ulexite from thermogravimetric data, J. Therm. Anal. Calorim. 48 (1997) 403–411.
[35] J.M. Criado, J. Morales, Defects of thermogravimetric analysis for discerning between first order reactions and those taking place through the Avrami–Erofeev's mechanism, Thermochim. Acta 16 (1976) 382–387.
[36] R. Ebrahimi-Kahrizsangi, M.H. Abbasi, Evaluation of reliability of Coats-Redfern method for kinetic analysis of non-isothermal TGA, Trans. Nonferrous Met. Soc. China 18 (2008) 217–221.
[37] E.K. Reza, M.H. Abbasi, A. Saidi, Model-fitting approach to kinetic analysis of non-isothermal oxidation of molybdenite, Iran. J. Chem. Chem. Eng. 26 (2007) 119–123.
[38] M. El-Husseiny, Diefallah, Kinetic analysis of thermal decomposition reactions: part VI. Thermal decomposition of manganese(II) acetate tetrahydrate, Thermochim. Acta 202 (1992) 1–16.
[39] M.A. Gabal, Kinetics of the thermal decomposition of CuC_2O_4–ZnC_2O_4 mixture in air, Thermochim. Acta 402 (2003) 199–208.
[40] B.N.N. Archar, G.W. Brindley, J.H. Sharp, Kinetics and mechanism of dehydroxylation processes, III. Applications and limitations of dynamic methods, Proc. Int. Clay Conf., Jerusalem 1 (1966) 67–73.
[41] J. Luo, K. Xu, M. Wang, J. Song, X. Ren, Y. Chen, F. Zhao, Syntheses and thermal behaviors of Rb(FOX-7)·H_2O and Cs(FOX-7)·H_2O, Bull. Korean Chem. Soc. 31 (2010) 2867–2872.
[42] C. Ma, J. Huang, Y.T. Zhong, K.Z. Xu, J.R. Song, Z. Zhang, Preparation, structural investigation and thermal decomposition behavior of two high-nitrogen energetic materials: ZTO·$2H_2O$ and ZTO(phen)·H_2O, Bull. Korean Chem. Soc. 34 (2013) 2086–2092.
[43] F.J. Gotor, J.M. Criado, J. Malek, N. Koga, Kinetic analysis of solid-state reactions: the universality of master plots for analyzing isothermal and nonisothermal experiments, J. Phys. Chem. A 104 (2000) 10777–10782.
[44] J.M. Criado, J. Malek, A. Ortega, Applicability of the master plots in kinetic analysis of non-isothermal data, Thermochim. Acta 147 (1989) 377–385.
[45] G.I. Senum, R.T. Yang, Rational approximations of the integral of the Arrhenius function, J. Therm. Anal. Calorim. 11 (1977) 445–447.
[46] L.A. Pérez-Maqueda, J.M. Criado, The accuracy of Senum and Yang's approximations to the Arrhenius integral, J. Therm. Anal. Calorim. 60 (2000) 909–915.
[47] A.I. Lesnikovich, S.V. Levchik, A method of finding invariant values of kinetic parameters, J. Therm. Anal. Calorim. 27 (1983) 89–93.
[48] P. Budrugeac, E. Segal, L.A. Pérez-Maqueda, J.M. Criado, The use of the IKP method for evaluating the kinetic parameters and the conversion function of the thermal dehydrochlorination of PVC from non-isothermal data, Polym. Degrad. Stab. 84 (2004) 311–320.
[49] D.M. Blake, L. Moens, D. Rudnicki, H. Pilath, Lifetime of Imidazolium salts at elevated temperatures, J. Sol. Energy Eng. 128 (2006) 54–57.
[50] D.A. Young, Decomposition of Solids, Pergamon Press, Oxford, UK, 1966, pp. 55–109.
[51] H.M. Cordes, Pre-exponential factors for solid-state thermal decomposition, J. Phys. Chem. 72 (1968) 2185–2189.
[52] J.M. Criado, L.A. Pérez-Maqueda, P.E. Sánchez-Jiménez, Dependence of the preexponential factor on temperature, J. Therm. Anal. Calorim. 82 (2005) 671–675.
[53] H. Eyring, The activated complex in chemical reactions, J. Chem. Phys. 3 (2) (1935) 107–115.
[54] C.N.R. Rao, B. Prakash, M. Natarajan, Crystal structure transformations in inorganic nitrites, nitrates, and carbonates, Nat. Stand. Ref. Data Ser., Nat. Bur. Stand. (U.S.) 53 (1975) 35–37.
[55] F. El-Kabbany, Y. Badr, G. Said, S. Taha, S. Mahrous, A study of the thermal hysteresis in $AgNO_3$, Phys. Status Solidi A 95 (1986) 127–134.
[56] H. Zamali, M. Jemal, Phase diagrams of binary systems: $AgNO_3$–KNO_3 and $AgNO_3$–$NaNO_3$, J. Phase Equilib. 16 (1995) 235–238.
[57] M. Hichri, C. Favotto, H. Zamali, Y. Feutelais, B. Legendre, A. Sebaoun, M. Jemal, Diagramme de phases du systeme binaire $AgNO_3$–$RbNO_3$, J. Therm. Anal. Calorim. 69 (2002) 509–518.
[58] B.V. L'vov, V.L. Ugolkov, Kinetics and mechanism of free-surface decomposition of solid and melted $AgNO_3$ and $Cd(NO_3)_2$ analyzed thermogravimetrically by the third-law method, Thermochim. Acta 424 (2004) 7–13.
[59] P. Pacák, H. Špalková, Crystal growth rate from the $AgNO_3$-dimethylsulfoxide melt, Cryst. Res. Technol. 19 (1984) 1175–1181.
[60] D.D. Wagman, W.H. Evans, V.B. Parker, R.H. Schumm, I. Halow, S.M. Bailey, K.L. Churney, R.L. Nuttall, The NBS tables of chemical thermodynamic properties, J. Phys. Chem. Ref. Data 11 (Suppl. 2) (1982).
[61] M. Makela, H. Keskinen, T. Forsblom, J. Keskinen, Generation of metal and metal oxide nanoparticle by liquid flame spray process, J. Mater. Sci. 39 (2004) 2783–2788.
[62] C. Haixiang, L. Naian, Z. Weitao, Critical study on the identification of reaction mechanism by the shape of TG/DTG curves, Solid State Sci. 12 (2010) 455–460.
[63] Y. Eom, S. Kim, S.-S. Kim, S.-H. Chung, Application of peak property method for estimating apparent kinetic parameters of cellulose pyrolysis reaction, J. Ind. Eng. Chem. 12 (6) (2006) 846–852.
[64] B.V. L'vov, Kinetics and mechanism of thermal decomposition of silver oxide, Thermochim. Acta 333 (1999) 13–19.
[65] B.V. L'vov, Application of the third-law methodology to investigation of decomposition kinetics, Thermochim. Acta 424 (2004) 183–199.
[66] H.-L. Feng, X.-Y. Gao, Z.-Y. Zhang, J.-M. Ma, Study on the crystalline structure and the thermal stability of silver–oxide films deposited by using direct-current reactive magnetron sputtering methods, J. Korean Phys. Soc. 56 (2010) 1176–1179.
[67] W.C. Sheets, E. Mugnier, A. Barnabé, T.J. Marks, K.R. Poeppelmeier, Hydrothermal synthesis of delafossite-type oxides, Chem. Mater. 18 (2006) 7–20.
[68] M. Erceg, T. Kovačić, S. Perinović, Kinetic analysis of the non-isothermal degradation of poly(3-hydroxybutyrate) nanocomposites, Thermochim. Acta 476 (2008) 44–50.
[69] P. Budrugeac, E. Segal, On the use of Diefallah's composite integral method for the non-isothermal kinetic analysis of heterogeneous solid-gas reactions, J. Therm. Anal. Calorim. 82 (2005) 677–680.
[70] K.H. Stern, E.L. Weise, High temperature properties and decomposition of inorganic salts, Nat. Stand. Ref. Data Ser., Nat. Bur. Stand. (U.S.) NSRDS-NBS 30, U.S. Government Printing Office, Washington, DC, 1969, pp. 1–32.
[71] N. Valim, Mechanistic Study of Silver Nitrate during the Selective Catalytic Reduction of NO_x with Ammonia over Ag/Al_2O_3 (Master of Science Thesis), Department of Chemical and Biological Engineering, Division of Chemical Reaction Engineering, Competence Centre for Catalysis, Chalmers University of Technology, Göteborg, Sweden, 2011, pp. 1–40.
[72] T. Morita, Y. Yasuda, E. Ide, Y. Akada, A. Hirose, Bonding technique using micro-scaled silver–oxide particles for *in-situ* formation of silver nanoparticles, Mater. Trans. 49 (12) (2008) 2875–2880.
[73] D.K. Lee, Y.S. Kang, Synthesis of silver nanocrystallites by a new thermal decomposition method and their characterization, ETRI J. 26 (3) (2004) 252–256.
[74] Z. Pesina, J. Sopousek, J. Bursik, Mechanical properties of joints created by silver nanoparticles, in: B. Katalinic (Ed.), Annals of DAAAM for 2012 & Proceedings of the 23rd International DAAAM Symposium, Vol. 23, No.1, DAAAM International, Vienna, Austria, EU, 2012, pp. 139–142, ISSN: 2304-1382.
[75] B. Ebin, E. Yazici, S. Gürmen, Production of nanocrystalline silver particles by hydrogen reduction of silver nitrate aerosol droplets, Trans. Nonferrous Met. Soc. China 23 (2013) 841–848.
[76] K.H. Stern, High temperature properties and decomposition of inorganic salts. Part. 3. Nitrates and nitrites, J. Phys. Chem. Ref. Data 1 (3) (1972) 747–772.
[77] B.V. L'vov, Theory of solid-state decomposition reactions: a historical essay, Spectrochim. Acta B 66 (2011) 557–564.
[78] A.B.D. Nandiyanto, K. Okuyama, Progress in developing spray-drying methods for the production of controlled morphology particles: from the nanometer to submicrometer size ranges, Adv. Powder Technol. 22 (1) (2011) 1–19.